T.C.
DOKUZ EYLUL UNIVERSITY
IZMIR INTERNATIONAL BIOMEDICINE AND GENOME INSTITUTE

INCREASING DIFFERENTIATION EFFICIENCY OF HUMAN INDUCED PLURIPOTENT STEM CELL DERIVED LACRIMAL GLAND ORGANOIDS

SUDE UYULGAN

MOLECULAR BIOLOGY AND GENETICS

MASTER OF SCIENCES THESIS

İZMİR-2022

Thesis ID: DEU.IBG.MSc. 2020850018

T.C.
DOKUZ EYLUL UNIVERSITY
IZMIR INTERNATIONAL BIOMEDICINE AND GENOME INSTITUTE

INCREASING DIFFERENTIATION EFFICIENCY OF HUMAN INDUCED PLURIPOTENT STEM CELL DERIVED LACRIMAL GLAND ORGANOIDS

SUDE UYULGAN

Supervisor: Assoc. Prof. Dr. Sinan GÜVEN

MOLECULAR BIOLOGY AND GENETICS

MASTER OF SCIENCES THESIS

İZMİR-2022

Thesis ID: DEU.IBG.MSc. 2020850018

Dokuz Eylül Üniversitesi İzmir Uluslararası Biyotıp ve Genom Enstitüsü Genom Bilimleri ve Moleküler Biyoteknoloji Anabilim Dalı, Moleküler Biyoloji ve Genetik Yüksek Lisans programı öğrencisi Sude Uyulgan **'INCREASING DIFFERENTIATION EFFICIENCY OF HUMAN INDUCED PLURIPOTENT STEM CELL DERIVED LACRIMAL GLAND ORGANOIDS'** konulu Yüksek Lisans tezini 21/06/2022 tarihinde başarılı olarak tamamlamıştır.

Doç. Dr. Sinan Güven
BAŞKAN

ÜYE

Doç. Dr. Hatice Güneş Özhan
Dokuz Eylül Üniversitesi

ÜYE

Doç. Dr. Melis Palamar Onay
Ege Üniversitesi

YEDEK ÜYE

Doç. Dr. Şerif Şentürk
Dokuz Eylül Üniversitesi

YEDEK ÜYE

Doç. Dr. Zeynep Fırtına Karagonlar
İzmir Ekonomi Üniversitesi

Dokuz Eylul University Izmir International Biomedicine and Genome Institute Department of Genomics and Molecular Biotechnology,

Molecular Biology and Genetics graduate program Master of Science student Sude Uyulgan has completed her Master of Science thesis titled ' **CREAS NG D FFERENTIAT ON EFFICIENCY OF HU AN NDUCED PLUR POTENT STEM CELL DERIVED LACR AL GLAND ORGANO DS'** on the date of 21/06/2022.

Assoc. Prof. Sinan Güven
HAIR

MEMBER

As

MEMBER

Assoc. Prof. Melis Palamar Onay
Ege University

SUBSTITUTE MEMBER

Assoc. Prof. Şerif Şentürk
Dokuz Eylul University

SUBSTITUTE MEMBER

Assoc. Prof. Zeynep Fırtına Karagonlar
Izmir University of Economics

TABLE OF CONTEXT

INDEX OF FIGURES

INDEX OF TABLES

LIST OF ABBREVIATIONS

2.5D	2.5-Dimensional
3D	3-Dimensional
α-SMA	α-Smooth Muscle Actin
AQP5	Aquaporin 5
aSC	Adult Stem Cell
BARX2	BARX Homeobox 2
BF	Bright Field
BMP7	Bone Morphogenic Protein 7
BSA	Bovine Serum Albumin
c-DNA	Complementary DNA
CE	Conjuctival Epithelium
CK	Cytokeratin
Col1a1	Collagen type I alpha-1 chain
Col2a1	Collagen type II alpha -1 chain
Col9a1	Collagen type IX alpha -1 chain
DAPI	4',6-Diamidino-2-Phenylindole, Dihydrochloride
DED	Dry Eye Disease
DM	Differentiation Medium
DMEM/F12	Dulbecco's Modified Eagle's Medium and Ham's F-12 Nutrient Mixture
ECM	Extracellular Matrix
EDM	Eye Field Differentiation Medium
EGF	Epidermal Growth Factor
ESC	Embryonic Stem Cells
FGFR2	FGF Receptor 2
FGFs	Fibroblast Growth Factors
FOCX1	Forkhead transcription factor
GAGs	Glycosaminoglycans
GAPDH	Glyceraldehyde 3-Phosphate Dehydrogenase
hiPSCs	Human Induced Pluripotent Stem Cells
HS	Heparan Sulfate

ICC	Immunocytochemistry
IF	Immunofluorescent
IHC	Immunohistochemistry
KSR	Knockout Serum Replacement
LCN	Lipocalin
LG	Lacrimal Gland
LGR5	Leucine-rich repeat-containing G-protein coupled receptor 5
LTF	Lactoferrin
MEC	Myoepithelial Cell
MMPs	Matrix Metalloproteinases
mRNA	Messenger RNA
MTG	Monothioglycerol
MZOC	Multi Zonal Ocular Cells
NAG	N-Acetylglucosaminidase
NDST1	N-deacetylase/N-sulfotransferase
NEAA	Non-Essential Amino Acids
OCT	Optimal Cutting Temperature
ODM	Ocular Cell Differentiation Medium
OSE	Ocular Surface Ectoderm
PAX6	Paired Box Protein 6
PBS	Phosphate Buffered Saline
PBS-T	Phosphate Buffered Saline-Tween 20
PFA	Paraformaldehyde
PMMA	Polymethyl Methacrylate
PSCs	Pluripotent Stem Cells
qPCR	Quantitative Polymerase Chain Reaction
Rocki	Rock inhibitor
SOX	SRY-Box Transcription Factor
Tm	Primer Melting Temperature
WT-1	Wild-type 1

ACKNOWLEDGEMENTS

Firstly, I'd like to express my gratitude to my thesis supervisor, Assoc. Prof. Sinan Güven, for allowing me to pursue my curiosity on stem cell research. His support and guidance were endless throughout my master's education. I am also truly thankful to my previous professors and mentors for not only guiding me to this point but also, teaching me how to do science and prepare myself for the future steps to come. I was supported by the TUBITAK 2210-A scholarship, for which I am grateful.

I would like to thank all the current Güven Lab members for their support and companionship on this journey, I will always remember this special friendship. My special thanks to İrem Duman for all the fun we had in and out of the lab, and Tuğba Topbaş for her amazing organizational skills (to the extent where she swipes the lab materials even before we begin the experiments) while providing endless support to our experiments, Elifsu Polatlı and Vedat Sarı for their contribution to this thesis with the microfluidics platform and metabolomics analyses, and Ali Can Koç for the friendship besides all the support. I would also like to thank all the members of IBG core facilities, especially Ece Uzun, for her patience and help in slicing every single small sample of mine.

Arda Kıpçak, I feel so lucky and grateful to have your continuous support, love, and patience. You helped me every time I felt lost and stressed, talked to me for hours, and found solutions to every problem I had. Thank you for always being there whenever I needed you, and for believing in me even when I did not. I would not have come this far without your endless help. Many thanks to my life-long friends, Yaren Gülce Yıldız and Dilay İlhan for always supporting me for all these years. Thank you Burçin Dersu Açıkgöz for your unwavering friendship.

Lastly, I would like to express my deepest gratitude to my parents, Berrin and Tamer Uyulgan for giving me endless support and help throughout my life. I dedicate this thesis to my beloved family, who gave me the chance and encouragement for taking a step in this journey and supported me for planning many more.

INCREASING DIFFERENTIATION EFFICIENCY OF HUMAN INDUCED PLURIPOTENT STEM CELL DERIVED LACRIMAL GLAND ORGANOIDS

Sude Uyulgan, Izmir International Biomedicine and Genome Institute, Dokuz Eylul University, 15 Temmuz Saglık ve Sanat Yerleskesi, Balcova, 35340, Izmir/Turkiye

ABSTRACT

The lacrimal gland (LG), also known as the tear gland, maintains homeostasis on the ocular surface by secreting electrolytes and proteins creating the aqueous layer of the tear film. As the main exocrine gland of the eye, it lubricates and protects the eye by the production of lacrimal fluid. Loss of function due to damage to the LG adversely affects eye health and vision quality. Although a large part of the human population is affected by eye diseases based on functional disorders in the LG such as dry eye disease, studies on human LG formation and development are limited.

The LG is a structure that develops by branching, and it reaches its structural and functional maturity only when this process is completed, similar to salivary or mammary glands. In this study, human induced pluripotent stem cells (hiPSCs) were differentiated into cells with characteristics of LG *in vitro* by recapitulating budding and branching morphogenesis. Branching was stimulated via exogenous FGF10 and BMP7 proteins aiming to increase the differentiation efficiency. As an additional approach, the LG models were developed under dynamic conditions using microfluidic platforms to better mimic the native environment and develop more realistic LG models.

In this context, the effects of this stimulation were examined at the RNA and protein levels of gene expressions. The results suggest that budding and branching development could be induced *in vitro* using exogenous supportive proteins. Additionally, developed models could be improved using dynamic conditions and these platforms could be used as a potential platform for therapeutic approaches.

Keywords: Human induced pluripotent stem cells, stem cell differentiation, lacrimal gland, dry eye disease, organoid

İNSAN İNDÜKLENMİŞ PLURİPOTENT KÖK HÜCRE KAYNAKLI LAKRİMAL BEZ ORGANOİDLERİNİN FARKLILAŞMA VERİMLİLİĞİNİN ARTTIRILMASI

Sude Uyulgan, İzmir Uluslararası Biyotıp ve Genom Enstitüsü, Dokuz Eylül Üniversitesi, 15 Temmuz Sağlık ve Sanat Yerleşkesi, Balçova, 35340, İzmir/Türkiye

ÖZET

Gözyaşı bezi olarak da bilinen lakrimal bez (LB), gözün dış yüzeyini kaplayan elektrolitleri ve proteinleri salgılayarak gözyaşı sıvısını oluşturur ve oküler yüzeydeki dengeyi korur. Bir ekzokrin bez olarak lakrimal bez, gözyaşı sıvısı üreterek gözün yüzeyinin nemli kalmasından sorumludur. LB 'nin hasar görmesi nedeniyle fonksiyon kaybının oluşması göz sağlığını ve görme kalitesini olumsuz etkiler. İnsan nüfusunun önemli bir kısmı kuru göz hastalığı gibi LB'de fonksiyonel bozukluklara dayalı göz hastalıklarından etkilenmesine rağmen, insan LB oluşumu ve gelişimi üzerine yapılan çalışmalar sınırlıdır.

LB, dallanarak gelişen bir yapıdır ve tıpkı tükürük bezleri veya meme bezleri gibi ancak bu süreç tamamlandığında yapısal ve işlevsel olgunluğuna ulaşır. Bu çalışmada, insan kaynaklı pluripotent kök hücreler (hiPSC'ler), tomurcuklanma ve dallanma morfogenezinin özetlenmesiyle in vitro LB özelliklerine sahip hücrelere farklılaştırılmıştır. Dallanma, farklılaşma etkinliğini arttırmayı amaçlayan eksojen FGF10 ve BMP7 proteinleri ile uyarım sağlanmıştır. Ek bir yaklaşım olarak LB modelleri, doğal ortamı daha iyi taklit etmek ve daha gerçekçi LG modelleri geliştirmek için mikroakışkan platformlar kullanılarak dinamik koşullar altında geliştirilmiştir.

Bu kapsamda gen ifadelerinin RNA ve protein seviyelerinde bu uyarının etkileri incelenmiştir. Sonuçlar, tomurcuklanma ve dallanma gelişiminin, ekzojen destekleyici proteinler kullanılarak in vitro olarak indüklenebileceğini göstermektedir. Ayrıca geliştirilen modeller dinamik koşullar kullanılarak iyileştirilebilir ve bu platformlar ileriki çalışmalarda terapötik yaklaşımlar için potansiyel bir platform olarak kullanılabilir.

Anahtar Kelimeler: İnsan uyarılmış pluripotent kök hücreleri, kök hücre farklılaşması, lakrimal bez, kuru göz hastalığı, organoid

1. INTRODUCTION AND GOALS

1.1. Statement and Importance of the Problem

The lacrimal gland (LG) is an exocrine gland located on the eyeball whose main function is to produce lacrimal fluid to maintain homeostasis on the ocular surface (Conrady et al., 2016). The LG plays an important role in eye health and vision quality via the fluid components (water, electrolytes, and proteins) it produces. The secretion is maintained through short channels, and ducts, to the outermost layer of the eye also called as the ocular surface, supporting and protecting the surface metabolism, corneal transparency and the quality of the of vision by creating a tear film (Garg & Zhang, 2017; Holly & Lemp, 1977; Johnson & Murphy, 2004). Stabilization of the tear film and the dynamic structure of the ocular surface is one of the most important elements required for healthy vision. Damages that can disrupt this structure have the potential to cause permanent damage on the visual sensory system (Lu et al., 2017).

Although a large part of the human population affected by eye diseases that are occur due to the loss of LG function such as dry eye disease, studies on human LG formation and development are limited. DED is a multifactorial disease of the ocular surface marked by a loss of tear film homeostasis and ocular symptoms (Craig et al., 2017). It can be occurred in various forms, and may lead to vision loss due to corneal epithelial cell damage. The current therapy options are not sufficient enough to cure the damage, most of them are temporary solutions focusing on increasing the comfort of the patient. Therefore, new solutions needed to cure DED.

It is now possible to generate *in vitro* models such as organoid models which can recapitulate the human organ development and improve them for therapy purposes with the enhances in the fields of tissue engineering and regenerative medicine. Organoid-based therapies taking advantage of stem cells are based on assisting in the acquisition and differentiation of functional cells that can lead to regeneration of damaged tissues. In this study, hiPSCs used differentiated to form LG organoids. As a gland, LG undergoes a process of branching morphogenesis similar to salivary and mammary glands before reaching structural and functional maturity. The branched structure provides the advantage of optimizing the functions by maximizing the surface

area within a limited space (C. H. Dean et al., 2005). Here, the branching structure is stimulated on organoids to advance the differentiation of hiPSCs to LG models.

1.2. Purpose of the Research

The purpose of this research is to increase the efficiency of existing human induced pluripotent stem cell derived lacrimal gland protocol by improving the culture conditions such as the development of 3-Dimensional (3D) organoid models and the use of dynamic microfluidic platforms, as well as providing supporting molecules to recapitulate the budding and branching morphogenesis *in vitro*.

1.3. Hypothesis of the Research

In this work, it is hypothesized that the budding and branching morphogenesis induced by supplementary molecules, increases the differentiation efficiency of hiPSCs into LG organoids. Moreover, this improved differentiation can be further complemented using microfluidic platforms. It is expected that the differentiation efficiency of the groups stimulated by supporting molecules will be higher relative to non-supplemented controls. Similarly, organoids that grow in dynamic culture conditions are expected to have an improved differentiation efficiency compared to static conditions.

2. GENERAL INFORMATION

2.1. Lacrimal Gland

Lacrimal gland (LG) is a tubuloacinar exocrine gland that is anatomically similar to mammary and salivary glands. (Garg & Zhang, 2017; Makarenkova & Dartt, 2015). LG is located on the upper part of the eye and is responsible for the formation of aqueous layer of the tear film as well as the protection of the ocular surface which consist of cornea and conjunctiva. By the tear formation, LG maintains the homeostasis of the ocular surface microenvironment and physiological function (Hirayama et al., 2016). Tears are mainly transfer oxygen and other nutrients to corneal and conjunctival cells while removing waste components from these cells. Therefore, LG has a critical role in eye health and vision quality.

The tear film generates a smooth layer over the cornea for a proper reflection of light, lubricates the ocular surface while supporting the metabolism and protects it from the external dirt and potential infections by releasing immunoglobulins (Garg & Zhang, 2017; Holly & Lemp, 1977; Johnson & Murphy, 2004). This film consists of three layers; mucous layer on top of the corneal epithelium, aqueous layer that is over 90% of the tear film by the volume, and lipid layer as the outermost part (Figure1). The mucous layer is produced by the goblet cells from conjunctiva and the stratified squamous cells of the cornea. This layer serves as a link between the ocular surface and the tear film, which contains mucins that help to prevent bacterial invasion and smooth out any abnormalities in the cornea. The lipid layer is responsible for protecting the lubricity of the surface, it prevents evaporation of the tears and is secreted via Meibomian glands that are located on both upper and lower eyelids (Downie et al., 2021; Makarenkova & Dartt, 2015).

The human LG is located in the upper temporal orbit, secretes mainly water, electrolytes and a limited number of proteins that are vital to the eye health (Walcott, 1998; Zoukhri et al., 2008). It has approximately 20x12x5 mm size in length, width and lobes respectively.

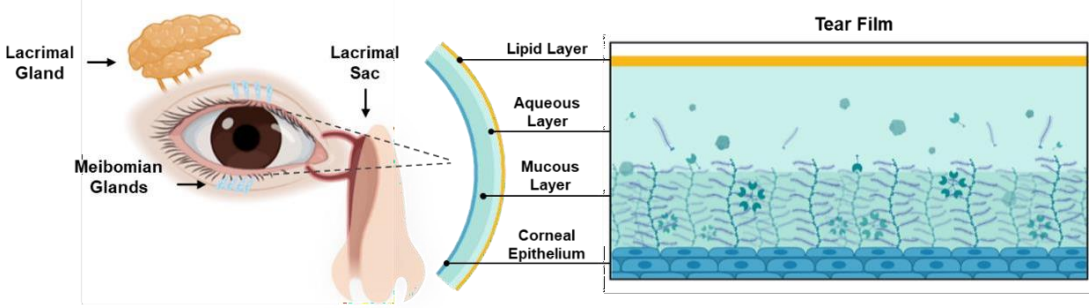

Figure 1. Schematic illustration of ocular glands and structure of tear film

The LG epithelium mainly consists of three cell types: acinar, ductal, and myoepithelial cells (Figure 2). 80% of the mass of the gland is composed of acinar cells which make up the primary secretory mechanism. These cells are responsible for synthesizing and secreting the proteins, electrolytes, and water which make up the tear. Acinar cells are surrounded by the cuboidal duct cells which account for 10-12% of the LG cell population and provide 30% of the LG secretions (Mircheff, 1989). The tight connections that surround the cells at the lumen, splitting the plasma membrane

into apical and basal membranes, facilitate unidirectional protein secretion from acinar cells. The transmitters and peptides are released in close proximity to the acinar cell membranes in the lacrimal gland, which is heavily innervated (Paulsen & Berry, 2006). Like acinar cells, ductal cells are connected to the apical side by tight junctions and support unidirectional flow by creating polarized cells. Ductal cells carry the tear from the acini to the ocular surface while maintaining the electrolyte composition before the exit. Although the duct cells also secrete proteins with a mechanism similar to acinar cells, they have fewer granules.

The myoepithelial cells (MECs) are localized around the acinar and ductal cells, responsible for maintaining the structural integrity and synthesizing the basal membrane (Downie et al., 2021). The basal membranes contain neurotransmitters and neuropeptides for stimulation of the secretion as well as ion channels and transport proteins for electrolyte and water secretion. MECs have various processes on their basal side including the contraction of surrounding acinar and ductal cells to promote the tear secretion process (Hodges & Dartt, 2003). Their primary purpose is to apply pressure to assist LG fluid flow from secretory cells into the duct with smooth muscle actin located (α-SMA) on the basal side (Dartt, 2009; Hodges & Dartt, 2003). The apical membrane also contains a different set of ion channels and transport proteins and serves as a site of fusion of the delivery granules that transport LG secretory proteins.

In addition to the acinar, ductal, and MECs, LG also contains fibroblasts, lymphocytes, plasma cells, macrophages, and mast cells that release histamines and matrix proteins. Thereby the immune protection on the ocular surface can be maintained. It has been shown that more than half of the mononuclear cells in the LG are plasma cells, with the majority of them being immunoglobulin A positive as it is one of the main components of the immune system of the ocular surface (Wieczorek et al., 1988).

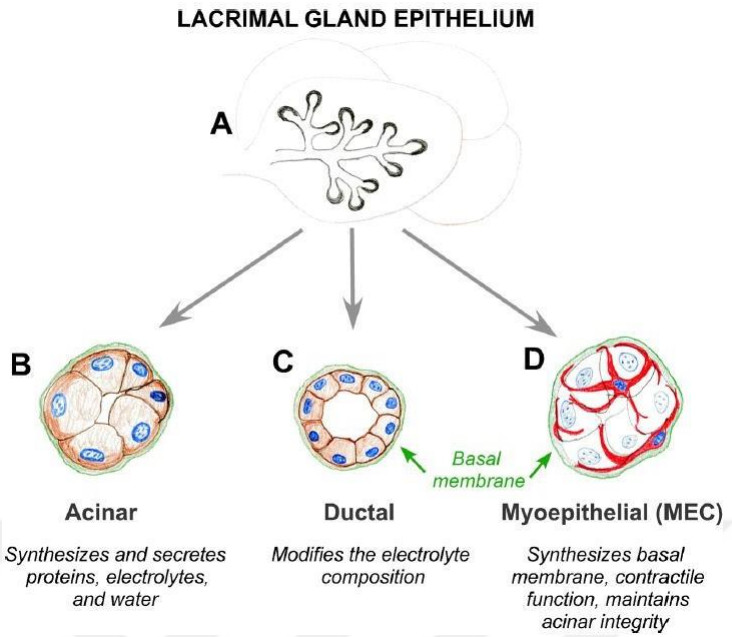

Figure 2. Cell types of lacrimal gland epithelium
A) The LG epithelium is consisting of, B) Acinar cells; C) Ductal cells; and D) Myoepithelial cells (MECs) (red) (Makarenkova & Dartt, 2015).

LG contains stem cells that undergo proliferation in case of repair or restoration of acinar cells (Dietrich & Schrader, 2020; Gromova et al., 2017; Tiwari et al., 2014). The exact location of these stem cells in the human lacrimal gland is unknown. As firstly identified in crypts of small-intestine, LGR5 stem cells has the potential to build crypt-villus structures (Sato et al., 2009). Although there are no reports in the literature on LGR5 expression in the lacrimal gland, its downstream element is β-Catenin highly active in salivary gland branching morphogenesis, implying a role in LG branching morphogenesis. (Patel et al., 2011).

2.1.2. Histology of The Human Lacrimal Gland

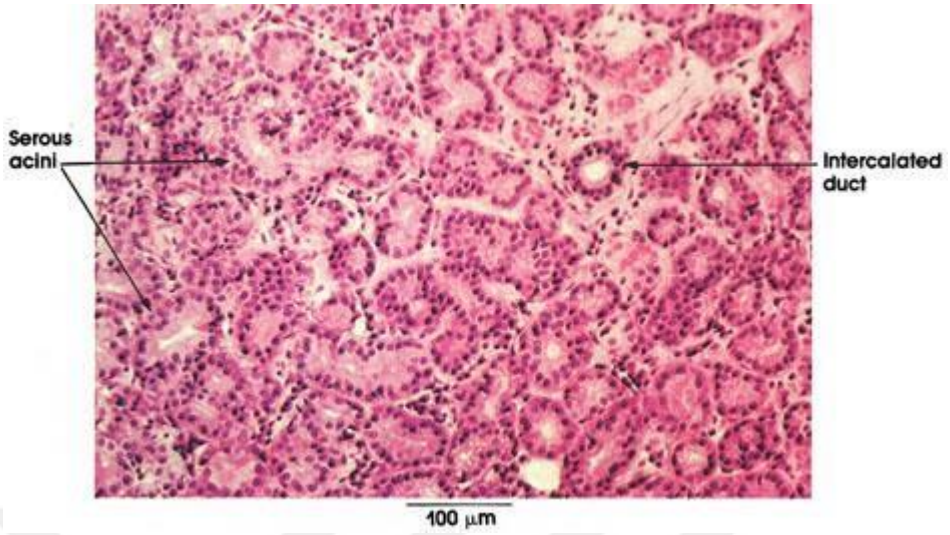

Figure 3. Histology of the human lacrimal gland
(Figure adapted from; *Anatomy Atlases: Atlas of Microscopic Anatomy: Section 1 - Cells*, n.d.)

The LG is made up of several lobules that are connected by loose connective tissue, where each lobule consists of acini and intercalated ducts. Interlobular ducts, veins, nerve fibers, fibroblasts, numerous plasma cells, and a few lymphocytes are all found in the connective tissue (Figure 3) (Obata, 2006). Tall cells with basal nuclei make form the serous acini. The apical cytoplasm is filled with various secretory granules while the basal portion of the cell contains endoplasmic reticulum and Golgi apparatus with the nucleus. Cuboidal cells line the duct cells in one or two layers. The basal side of the duct cells is connected by gap junctions while they are apically connected with tight junctions to generate a unidirectional flow of the tear fluid. Similar to acinar cells, the nucleus of the duct cells is located at the basal portion. The endoplasmic reticulum and Golgi apparatus are found in more apical locations (Paulsen & Berry, 2006).

2.1.3. Induction of Tear Secretion

Neurotransmitters and growth factors, as well as peptide and steroid hormones, have all been proven to promote LG fluid secretion. Multiple signaling pathways are activated by these stimuli and leading to tear secretion. It has been proven that acinar cells are stimulated via numerous hormones including but not limited to, retinoic acid,

prolactin, androgens, estrogens, glucocorticoids, growth hormones, thyroid stimulating hormone, insulin, vasopressin (Sullivan, 2004).

Even though water, protein, and electrolyte secretion from the LG are highly regulated by different mechanisms, they are all controlled via tight neural regulation. The LG functional unit consists of sensory afferent nerves of the ocular surface and the efferent nerves (parasympathetic and sympathetic) that innervate the LG secretory cells and excretory ducts (Figure 4). Once a plethora of afferent sensory nerves are stimulated, they activate efferent nerves to stimulate secretion of the LG fluid from ducts onto the ocular surface. The sensory input is reached to central nervous system to be processed at the brain's lacrimal nucleus, where also other inputs are processed such as emotional inputs. Thereby, a graded output is generated, so that the levels of sensory nerve stimulation determine the produced LG fluid volume. Likewise, intense stimulations such caused by emotions or exposure to foreign substances on the ocular surface leading to increased LG fluid levels and producing overflow tears (Dartt, 2009).

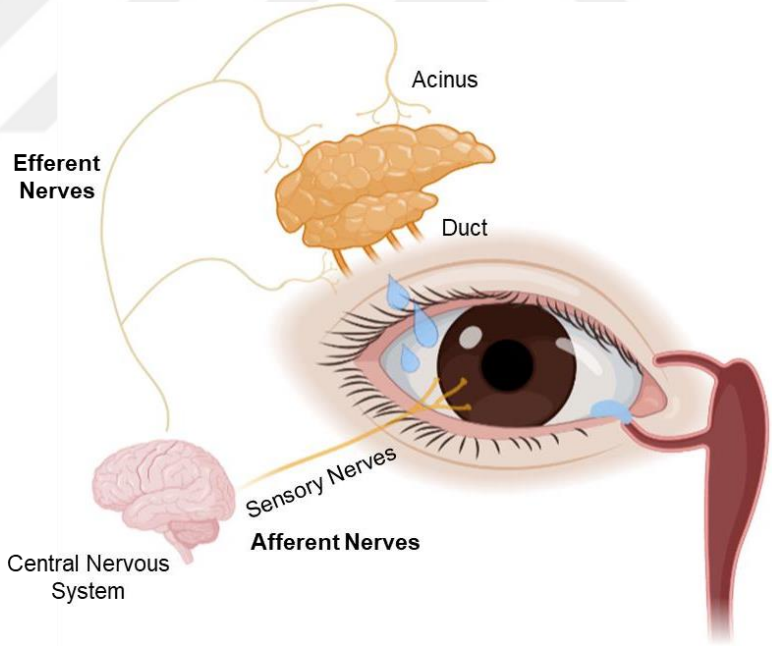

Figure 4. Neural stimulation of lacrimal gland
The afferent sensory neurons from the conjunctiva and cornea induce secretion. Efferent nerves innervate the acinar and ductal cells and induce secretion. Lacrimal fluid drains through the ducts and hydrates the ocular surface.

Tear flows through a duct system to reach the ocular surface, outflow components are found on the nasal side of the eye, where puncta on the upper and lower lids drain fluid into canaliculi that go to the lacrimal sac (Figure 4)(Walcott, 1998). Blinking mechanism produces enough force to push the secreted tear over the ocular surface (Doane, 1981).

Electrolyte and water secretion from LG is driven by the efflux of Na^+, and influx of K^+ across the apical membrane by the energy produced by Na^+, K^+ ATPase (Figure 5). On the basolateral membrane, the energy of inward NA^+ is used by the Na^+/H^+ and Cl^-/HCO_3^- exchangers and the Na^+-K^+-$2Cl^-$ symporter to support the influx of Cl^-. As a result of the Cl^- influx, a favorable Cl^- efflux is generated on the apical side, which establishes a potential difference in the lumen. This difference results in K^+ selective channel activation, thereby supporting the production of Na^+-Cl^- rich fluid production by acinar cells.

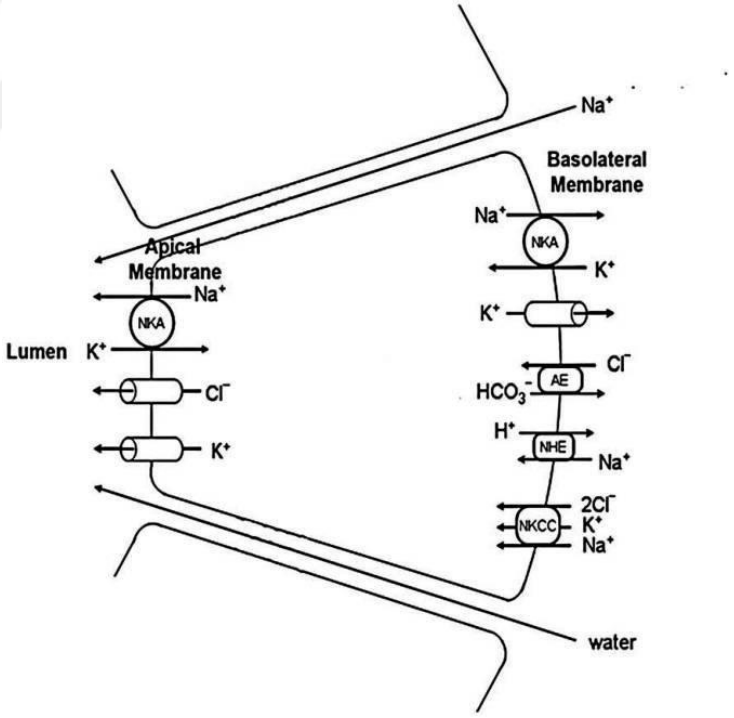

Figure 5. Mechanism of secretion of lacrimal gland acinar cells
(Dartt, 2009)
Electrolyte and water transport through the membrane is maintained by channel proteins.

2.2. Development of the Lacrimal Gland

Similar to mammalian embryogenesis, epithelial-mesenchymal interactions play a critical role in the development of human LG. Especially, interactions between the conjunctival epithelium and the periocular mesenchyme culminate in the formation of the LG. The development of LG in humans begins with the thickening of the conjunctival epithelium (CE) which then invades the mesenchyme to form branching cords (Figure 6) (de la Cuadra-Blanco et al., 2003; Garg & Zhang, 2017). Mesenchymal cells that surround the epithelial bud are coming from neural crest origin (Johnston et al., 1979). The gland maturates at around weeks 9-16, by forming a branched structure with acini and secretory granules, which gives a lobular structure to the mature gland (Kammandel et al., 1999).

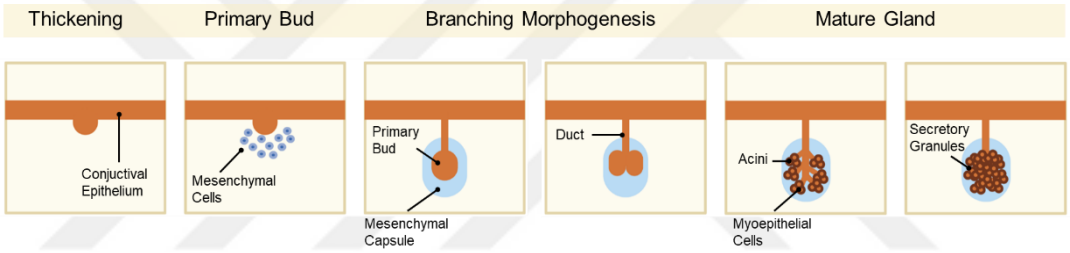

Figure 6. Lacrimal gland morphogenesis
LG development starts with the thickening of the conjunctival epithelium, which is then surrounded by invading mesenchymal cells. Ducts form within the mesenchymal capsule and give rise to acini, myoepithelial cells, and secretory granules.

A plethora of signaling pathways play an important function in LG development (Figure 7). The initiator signals for LG budding and branching morphogenesis are fibroblast growth factors (FGFs), dominantly FGF10 and FGF7. FGF10 is mainly expressed in the mesenchymal cells located around the epithelial bud whereas FGF7 expression is more distributed in the mesenchyme (Makarenkova et al., 2000, p. 10). They both can bind to fibroblast growth factor receptor-2 (FGFR2) and signal through the regulation of SRY-Box Transcription Factor (SOX) 9 and SOX10 expression (Chen et al., 2014).

Release of FGF10 from proteoglycans is facilitated by the expression of two matrix metalloproteinases, MMP2 and MMP9 that are secreted into the mesenchyme via the stimulation of the transcription factor BARX2 in the LG epithelium (Tsau et al.,

2011). This process provides a positive feedback mechanism for modulating Fgf10 concentrations before the epithelial bud invades.

Apart from its transcriptional level, the concentration of FGF10 protein in the periocular mesenchyme is exquisitely regulated by proteoglycans in the extracellular matrix (ECM). Qu and his colleagues have shown that glycosaminoglycans (GAGs) restrict the diffusion of FGF10 in the periocular mesenchyme during LG development, thereby inducing significant FGF signaling to trigger bud formation in the epithelium. Moreover, they have suggested that heparan sulfate (proteoglycan) modification enzymes *N*-deacetylase/*N*-sulfotransferase (Ndst1/2) are playing a role in the regulation of localization of FGF10 (Qu et al., 2012).

Paired box protein-6 (Pax6) has been discovered as a competent factor for LG formation as one of the key transcription factors expressed in the eye. Pax6 is mainly expressed in the conjunctival epithelium, and any mutations in this gene can result in vision problems (Makarenkova et al., 2000, p. 10).

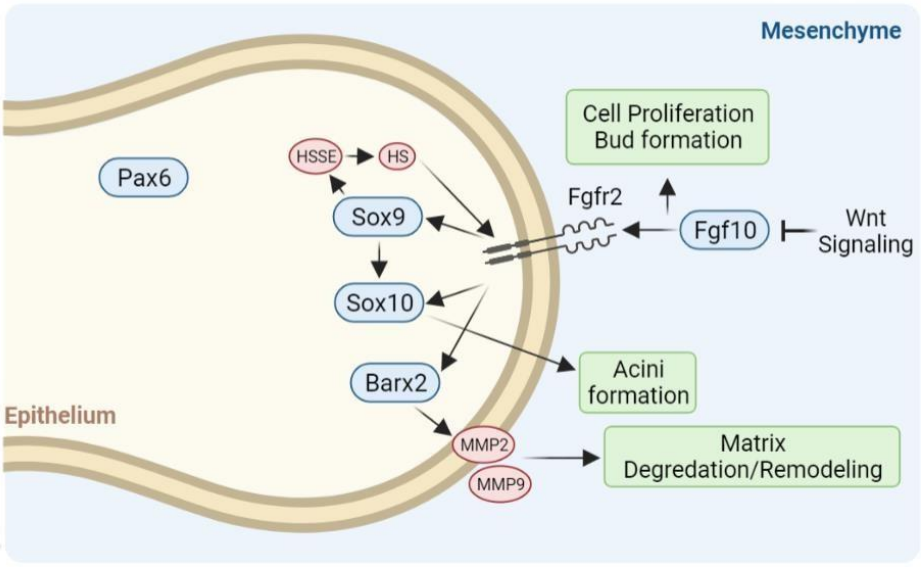

Figure 7. Signaling pathway interactions during lacrimal gland development

FGF10 stimulates molecules in the epithelium SOX9, SOX10 and BARX2 by binding to Fgfr2. SOX9 can activate both HSSE and SOX10 which triggers acini formation. The stimulated HHSE forms a positive feedback mechanism that enhance FGF activity, leading to cell proliferation and bud formation. The activation of the transcription factor BARX2 stimulates MMP activation to remodel the ECM.

2.1.1. Branching Morphogenesis

The LG develops via branching morphogenesis. The branching form has the benefit of optimizing functions by increasing the surface area in a restricted space. Branching morphogenesis in the LG begins with epithelial specification, followed by induction and elongation of the epithelial bud and at the and it formed mature gland by the bud and cleft formation (Tsau et al., 2011, p. 2). The outgrowth of the LG germ and branching morphogenesis is mainly controlled by ECM, receptors located on the ECM (FGF receptors), and ECM-remodeling enzymes such as MMPs. Makarenkova and colleagues showed that the changes in the FGF gradient govern branching patterns together with the morphogenetic gradient and downstream responses are regulated by the interactions between growth factors and heparan sulfates (HS) (Makarenkova et al., 2009).

Progression of branching morphogenesis requires the exchange of signals between epithelium and mesenchyme (Figure 8). It has been found that bone morphogenic protein (BMP) 7 regulates the process of branching, and in the absence of BMP7, the LG gland size reduces with a decrease in the branch number. BMP7 expression initially takes place in the periocular mesenchyme, which is then expressed in both epithelium and mesenchyme of LG. However, the primary target of the BMP7 is the mesenchyme where it stimulate increased cell division, and aggregation which triggers the upregulation of cadherins, connexin 43, and α-smooth muscle actin (α-SMA) (C. Dean et al., 2004, p. 7). Transcription of BMP7 has been found in association with forkhead transcription factor (FOXC1), as Foxc1 null mice showed a similar morphology with BMP7 null mice by reduced LG size and limited terminal cells (Mattiske et al., 2006). Indicating that, FOXC1 mediates the BMP signaling which is essential for LG development and branching morphogenesis.

Canonical Wnt signaling on the other hand, negatively regulates the branching by inhibiting the effects of FGF10 and BMP7. Thus, it regulates the shape and structure of the lacrimal gland (C. H. Dean et al., 2005). LGR5, an adult stem cell marker, is also a receptor protein that provides positive regulation of this canonical Wnt signaling (Kumar et al., 2014, p. 5). Even though not much is known about LGR5 role in LG branching development, in a recent study transcriptome analysis of lacrimal gland

organoids showed an increase in LGR5 expression under growth conditions (Bannier-Hélaouët et al., 2021).

Sox9 regulates the expression of col2a1 and col2a9 -the main collagens in the cartilage matrix- during the LG development. As most of the ECM components such as laminins, glycoproteins, and proteoglycans, including cell adhesion molecules stimulated through BARX2 expression, the collagens such as Col2a1 and Col9a1 are essential for LG branching morphogenesis (Chen et al., 2014; Daley & Yamada, 2013; Kim & Nelson, 2012).

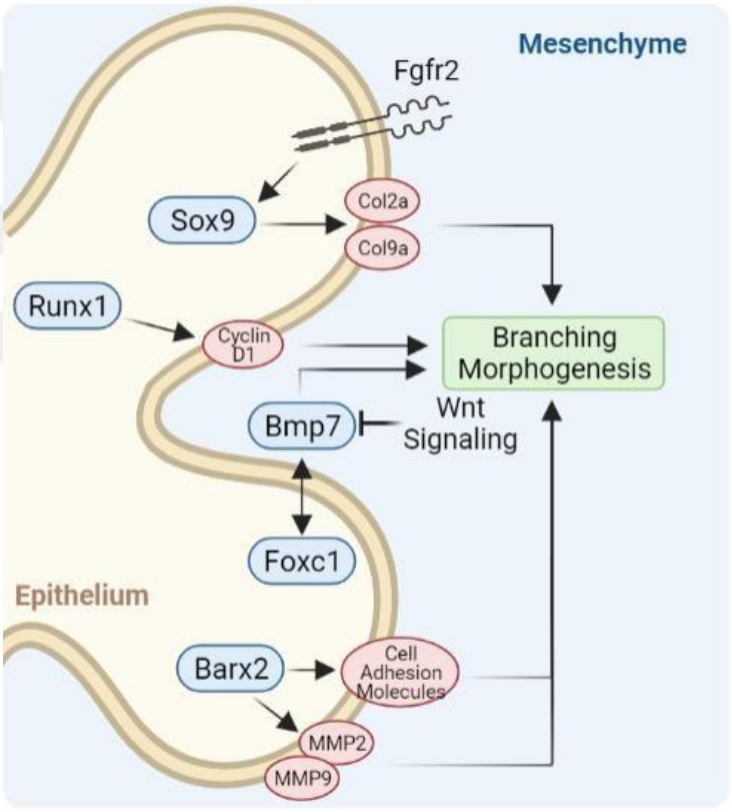

Figure 8. Signaling pathway interactions during lacrimal gland branching morphogenesis
BMP7 and FOXC1 interaction mediate signaling in the mesenchyme. Collagens (col9a, col2a), cell adhesion molecules, matrix metalloproteinases (MMP2, MMP9) and Cyclin D1 play an inductive role in bud formation and branching morphogenesis.

2.2. Dry Eye Disease

Tear protects the ocular surface from potential infections by releasing antimicrobial proteins such as lactoferrin, lipocalin, and lysozyme. These proteins are also important for regulating the function of the cells found in the cornea and conjunctiva (Hodges & Dartt, 2003). Any alterations in the tear electrolytes have been correlated with dry eye syndrome which can lead to deleterious effects on vision quality and health (Figure 9). It is defined by TFOS DEWS II as a multifactorial disease of the ocular surface marked by a loss of tear film homeostasis and ocular symptoms in which tear film instability and hyperosmolarity, ocular surface inflammation and injury, and neurosensory abnormalities all play etiological roles (Craig et al., 2017). The prevalence of dry eye disease (DED) worldwide is estimated at around 5% to 50%, varies greatly between populations and studies; increases with age (Donthineni et al., 2019; Stapleton et al., 2017; Wan et al., 2019).

DED is subdivided into two forms in clinics: aqueous deficient DED which is also known as the dry eye with reduced tear production and hyperevaporative DED which is the dry eye with increased evaporation of the tear film (Messmer, 2015). More than 80% of the cases are in mixed form (hyperevaporative/aqueous-deficient) (Lemp et al., 2012; Messmer, 2015).

Hyperevaporative DED is primarily a cause of meibomian gland injury. As the meibomian gland is crucial for maintaining the lipid layer of the tear film's homeostasis, a malfunction in this gland results in decreased lipid component production and therefore, thinning of the lipid layer. Lipid layer's disappearance exposes the aqueous layer to the atmosphere which then leads to rapid evaporation on the ocular surface. Broken tear film eventually results in DED. Besides, aqueous deficient DED is mainly caused by LG injury. Due to the dysfunction of LG, tear secretion is reduced, causing the tear film dries down and the ocular surface to become unstable. The instability and hyperosmolarity stimulate an inflammation on the ocular surface leading to autoimmune diseases. Nonetheless, the loss of tear film endangers corneal epithelial cells to environmental threats. The damage that occurs on corneal epithelial cells causes pain in the eye, and ocular discomfort, reduces life quality, and even may lead to vision loss (Hirayama et al., 2013; Yao & Zhang, 2017).

LG dysfunction can be derived from a variety of factors such as systemic disorders like Sjögren's syndrome, or long visual activities, long term excessive use of contact lenses, low humidity environments, and aging (Hirayama et al., 2015). Sex and hormones also play a significant role in the pathogenesis of the LG, as DED predominantly develops in females (Sullivan, 2004). Moreover, anxiety problems and depression have been found strongly linked to DED (A et al., 2013). Sjogren's syndrome is the most prevalent and dangerous among these conditions. In the patients with Sjogren's syndrome, nerves that are responsible for secretory functions have reduced intensity and sensitivity, therefore the secretion ability of LG is dramatically diminished. With the reduced tear secretion, the tear's osmotic pressure is increased continuously and as a result, leads to DED (Dartt, 2009; Pflugfelder et al., 1999; Yao & Zhang, 2017).

2.2.1. Treatment Methods for DED

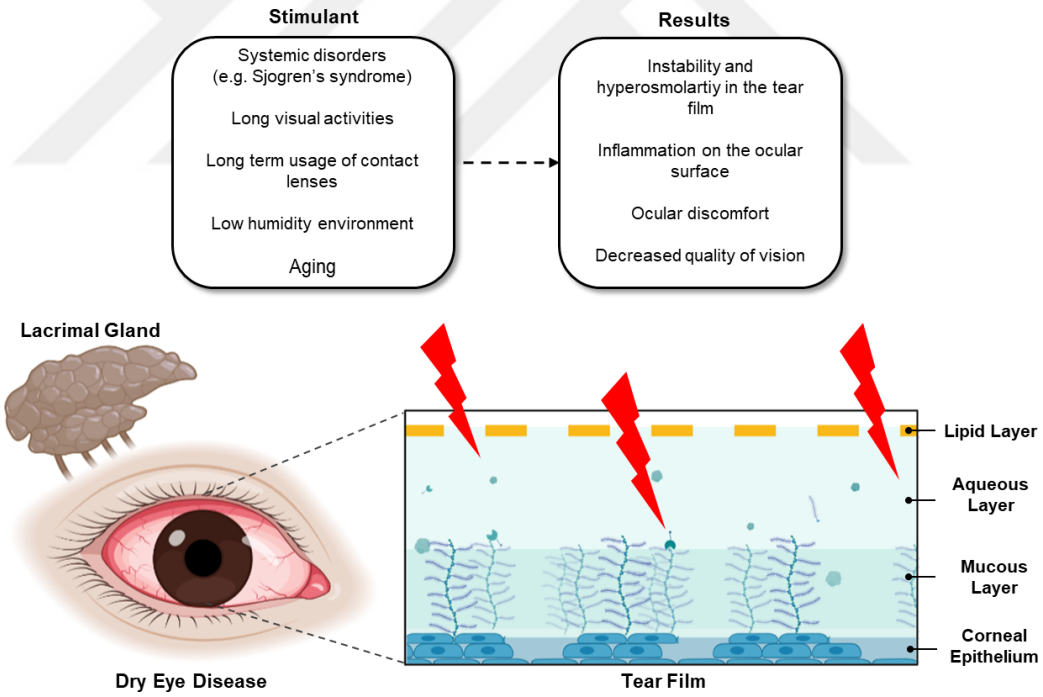

Figure 9. Dry eye disease
Dry eye disease can be caused by a variety of factors that disrupt the homeostasis on the ocular surface. The deteriorated tear film may progress until external factors damage the cornea epithelium.

Since DED occurs in different forms, there are a variety of treatments that are used to manage this disease. Despite this variety, the main purpose of the treatment is to restore the homeostasis of the tear film (Nelson et al., 2017). Most of the traditional treatments concentrate on relieving the pain and decreasing the discomfort of the patient. Artificial tear eye drops are commonly used in traditional treatment to moisten the ocular surface and provide extra lubrication as well as reduce ocular stress (Song et al., 2017; Tsubota et al., 1996). They are supposed to mimic tears and hence contain water, salts, proteins, and lipids, however, they are lacking in components. Some autologous serum drops are derived from blood, therefore they also contain growth factors such as plasma rich in growth factor, vitamins, and fibronectins aiming for a more efficient therapeutic effect on the ocular surface (Celebi et al., 2014). Nevertheless, its use is limited due to impractical acquisition and storage conditions. Besides eye drops, warm compresses and lid hygiene are used to treat DED. However, these treatments only provide temporary comfort, not a long-term solution. Furthermore, in severe forms of DED, such as aqueous deficient DED, these types of treatments remain inadequate to balance the homeostasis on the ocular surface, thereby they are insufficient to ease the symptoms.

Additionally, anti-inflammatory and topical immunosuppressive medications are used to treat chronic inflammation symptoms. For example, topical cyclosporin A is used for almost 20 years as an anti-inflammatory agent as it decreases T cell activation (O'Neil et al., 2019). However, because of their side effects such as ocular burning, conjunctival hyperemia, and visual disturbance, the persistent use is highly limited (Bron et al., 2017).

As one of the therapeutic approaches to restore the LG function, ectopic salivary gland transplantation *in vivo* has been reported and suggested as a promising regenerative medicine approach (Marinho et al., 2010; Sant' Anna et al., 2012). However, this therapy does not focus on the pathophysiology of aqueous deficient DED, so it is only a temporary solution. Also, saliva has a risk of causing epithelial defects by causing microcystic corneal edema due to its hypoosmolar secretion (Su et al., 2015). Moreover, their application has been limited due to the complex surgical process and possible complications.

Despite the increasing number of new therapeutic strategies for treating DED, there is still a need for an effective, long-term, and novel therapy alternative. Stem cells and their use in tissue engineering and regenerative medicine is a growing research topic with potential benefits for clinics as well.

2.3. Induced Pluripotent Stem Cells

Stem cells, the building blocks of life, are also called undifferentiated cells which are characterized by their ability to differentiate into any type of cell (potency) in our body and by their self-renewal capacity. These characteristics vary among stem cells, developmental potency is reduced with each phase. The very first cell formed after fertilization is the zygote, which has the highest differentiation potential, and totipotency. At this stage, cells can differentiate further, while forming the placenta. Embryonic stem cells (ESCs) are present in the inner cell mass of blastocyst which develops by the formation of three germs layer, the structure formed by pluripotent stem cells (PSCs). PSCs can differentiate into the cells that form all three germ layers, but not the placenta (Chagastelles & Nardi, 2011; Kolios & Moodley, 2013).

ESCs have become the key for cell-based therapy studies for human diseases with their differentiation capacity (Ramirez et al., 2010). However, the use of ESCs in therapeutic applications has major drawbacks such as ethical issues regarding on destruction of human embryos and finding the human leukocyte antigen (HLA) compatible ECSs need in medical applications (Bai et al., 2013; Landry & Zucker, 2004).

Although the cells with pluripotency only formed in blastocyst naturally, it is now possible to induce differentiated cells to revert to their pluripotent state with a process called reprogramming. The Nobel prized Yamanaka and colleagues report the method of reprogramming firstly in 2006, where they dedifferentiate mouse fibroblast cells into ESCs. They have induce the reprogramming through introducing ectopic expression of four genes, Oct4, Sox2, Klf4, and c-Myc (Takahashi & Yamanaka, 2006). Later on, they have successfully generate human iPSCs (hiPSCs) from adult human dermal fibroblasts with the same factors (Takahashi et al., 2007a). The produced iPSCs have similar features to natural pluripotent ECSs in terms of morphology, proliferation and *in vitro* differentiation patterns, gene expression, epigenetic status, telomerase activity,

and teratoma formation (Chin et al., 2010; Doi et al., 2009; Guenther et al., 2010; Mikkelsen et al., 2008; Takahashi et al., 2007b).

There are various methods for reprogramming somatic cells into iPSCs. Retroviruses are commonly used for genomic integration of exogenous genes into somatic cells. Once the virus integrates the cell genome, the cell's character differs depending on the given factors. However, because of its risks, other types of viruses such as adenovirus or sendaivirus also is used in some studies as non-integrating options (Ye et al., 2013). Furthermore, there are non-viral infection methods without genomic integration have been reported. For this purpose different non-viral methods have been developed such as, plasmids containing the factors cDNAs were given for transfecting cells, nonviral minicircle DNA vectors given to cells by repeated transfection or synthetic mRNA expressing the factors used (Narsinh et al., 2011; Okita et al., 2008; Warren et al., 2010).

Intensive attempts are being made to improve the efficiency of reprogramming and to create iPS cells with genetic changes as fewer as possible. Aside from reprogramming vectors and factors, the origin tissue of iPS cells has an impact on reprogramming efficiency.

2.4. Tissue Engineering and Organoid Models as Therapeutic Approaches

The major goal of tissue engineering is to develop and create replacement organs or tissues that can be transplanted under the right conditions to help the injured organ or region heal and regenerate faster (Langer & Vacanti, 1993). Various studies have been conducted on animal models *in vivo* including but not limited to Drosophila, rodents, or zebrafish models, or at cellular levels on cell culture models *in vitro* to improve tissue engineering approaches. However, due to differences between species, these studies may have limited in terms of clinical translatability. Additionally, *in vitro* models are most often unable to replicate organ-level functionality, which is required for recapitulating disease modeling. Thereby, more realistic models are required.

In response to this need, organoid technologies have been developed. Organoids are three-dimensional (3D) assemblies made from stem cells that are made up of organ-specific cell types that self-organize, simulating the architectural and functional complexity of native organs. Thereby, nowadays organoid technology can recapitulate human organ development and numerous human diseases 'in a dish'. Organoids can be derived from embryonic stem cells (ESCs), induced pluripotent stem cells (iPSCs) or organ-restricted adult stem cells (aSCs). Therefore, the generation of organoid models takes advantage of normal stem cells' seemingly limitless growth potential in culture. The differentiation of stem cells can be manipulated through supplementation of biological factors such as exogenous growth factors, ECM substrates, or small molecules to stimulate the fetal environment and support organoid maturation (Clevers, 2016). The developed models can then be used in various studies such as disease modeling, drug testing, and organ replacement (Figure 10).

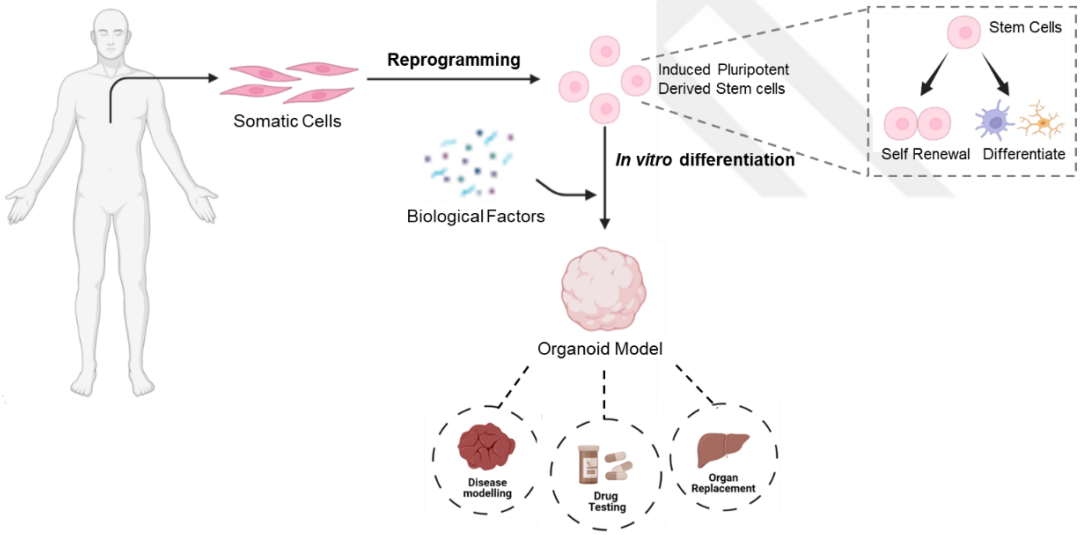

Figure 10. Human induced pluripotent stem cell derived organoid models

2.4.1. Lacrimal Gland Organoid Models

LG, like the other secretory glands, have the ability to self-renew after an injury. The regenerative capacity maintains throughout the lifetime, which is controlled by the stem cells (Dietrich & Schrader, 2020; Zoukhri et al., 2008). In recent years, many studies use stem cells to support tissue regeneration after injury and to restore the

function of the LG. In ophthalmology, regenerative medicines have progressively advanced to overcome vision-threatening eye disorders.

Recently, bioengineered LG germs have been developed using embryo-derived stem cells to regenerate LG. The mouse LG progenitor cells (epithelial and mesenchymal cells) are collected and placed in a collagen gel matrix to reconstruct LG germs *in vitro*. They have successfully maturated the LG germs and epithelial and mesenchymal interactions as similar to natural tissues with this method and showed tear-secretion function after engraftment to the aqueous deficient mouse *in vivo* (Hirayama et al., 2013; Nakao et al., 2007).

In another study focusing on human LG organoid formation, LG cells were collected from the patients, and after digestion, cultured in 3D conditions with the support of certain biological factors such as epidermal growth factor (EGF) and FGF. They have generated human free-floating spheres called “lacrispheres” under certain circumstances with acinar and ductal cells as well as quantifiable levels of tear proteins (Tiwari et al., 2018). This study showed promising findings for the ability of 3D culture of LG with a secretory function. Furthermore, previous studies have used biohybrid materials like decellularized scaffolds, to produce complicated secretory gland structures for a successful 3D reconstruction of LG (Lin et al., 2016; Spaniol et al., 2015).

In one of the latest studies, cells were harvested from human LG tissues both healthy and with Sjogren’s syndrome patients, cultured as a mixture with Matrigel in different culture mediums to stimulate organoid development. Formed organoids were tested against gene expression markers and tested for secreted proteins. As result, both the healthy and diseased organoids showed similar features histologically and functionally to normal and diseased tissues respectively (Jeong et al., 2021). Furthermore, recently a study was performed on generation of 3D LG organoids from different iPSCs by inducing supplementary molecules. They have been shown that the hiPSCs have the ability to differentiate into LG organoids with similarities to native LGs (Hayashi et al., 2022).

With the development of induced pluripotent stem cells, the development of organ-like structures in regenerative medicine and tissue engineering has been

expanded. As a result, the development of *in vitro* 3D culture models using iPSCs has gained widespread interest as a way to overcome the limitations of other approaches.

2.5. Organ-on-Chip Systems and Microfluidic Platforms

Organ-chip systems are cutting-edge platforms that integrate bioengineering and cell culture techniques to provide *in vitro* organ-like structures with in vivo-like functions and physiology on a micro-scale. These systems are designed to mimic the microarchitecture of the organs as well as their function in a dynamic environment. Microfluidic chips are the most effective systems for creating both physical/mechanical stimulations and biochemical gradients, in which tissues formed *in vitro* can be precisely controlled. Generally, these platforms consist of hollow microfluidic channels to allow the passage of the flow throughout the cell compartment (Manafi et al., 2021).

Many organs including the liver, gut, kidney, and lung have been modeled using organ-on-chip platforms. Additionally, just recently, eye structures such as the retina, cornea, and lens, or shortly the ocular surface, were added to the list (Seo et al., 2019; Xinaris et al., 2015). The chip developed by Seo et al., which merged both cornea and conjunctiva structures in the very same platform and integrated them with a blinking eyelid, was a significant step in the creation of an ocular surface chip. The device's tear secretion rate was adjusted to match natural values, and for the flow of the tear, a drainage system was created. Therefore, a uniform and thin tear film is maintained. They have modeled DED on this platform by reducing the blinking rate and humidity of the environment (Seo et al., 2019). These findings are extremely encouraging, and they pave the way for the development of chip-based models for a variety of additional ocular surface diseases.

3. MATERIALS AND METHODS

3.1. Type of Research

This research is an *in vitro* experimental research.

3.2. Date and Location of the Research

The research is conducted between October 2020 – May 2022 in Izmir Biomedicine and Genome Center (IBG).

3.3. Universe and Sample of the Research

This research was conducted via human induced pluripotent cells.

3.4. Materials of the Research

Wild type hiPSCs are reprogrammed in the laboratory of Assoc. Prof. Tamer Önder at Koç University (Istanbul, Turkey) were obtained from Prof. Dr. Esra Erdal at IBG Center (Izmir, Turkey).

3.5. Variables of the Research

Independent variables: Differentiation medium components, supplementary exogenous molecule concentrations, Matrigel concentrations, duration of the cell culture.

Dependent variables: Expression levels of the marker RNA and proteins, heterogeneity of the differentiated cells, cell morphology, and capacity to be subcultured.

3.6. Data Collection Methods

3.6.1. hiPSCs Differentiation into MZOC and Characterization

3.6.1.1. Culture of hiPSCs

WT1 human induced pluripotent stem cells (hiPSCs) which are generated as explained by Akbari et al., were cultured using complete mTeSR1 media (STEMCELL Technologies, 85851) at 37 °C, 5% CO_2 (Akbari et al., 2019). The medium was prepared by mixing the mTESR basal medium with its 5X supplement (STEMCELL Technologies, 85852) in a 4:1 (v:v) ratio. In order to maintain the pluripotent state, the medium was refreshed every day, and cells were passaged every 7 days or less depending on their confluency. hiPSC colonies were continuously monitored using a bright field microscope for their quality. The differentiated colonies were detected by their morphologies during the culture period, scraped, and removed from the environment by sterile pipette tips. Cells were plated on 1% Matrigel (Corning, 354277) coated wells, generally on 6-well sterile culture plates.

To prepare Matrigel coated plates, for one well of the 6-well plates, 12-13 µL Matrigel (varies depending on the LOT) mixed with 1 mL of serum-free Dulbecco Modified Eagle's Medium and Ham's F-12 Nutrient Mixture (DMEM/F12) (Gibco, Thermofisher Scientific, 31330) on ice. Since the Matrigel is gelled with temperature, and thaw at 4 °C, it was kept on ice during preparation for coating. The prepared 1% Matrigel solution was then immediately dispensed by 1 mL per well of the 6-well plate. After the mixture was transferred to the wells, the plate was incubated at 37 °C for 1 hour. After 1 hour of incubation, the plate was used for cell cultivation.

To passaged hiPSCs, first, the differentiated cells were removed from the culture by scraping, then the medium aspired. The well was washed with 1mL of DMEM/F12. 1 mL of ReLeSR (STEMCELL Technologies, 05872) was added to the empty well and incubated for 1 min at room temperature (RT). The ReLeSR was removed, and the empty well was then incubated for 4 min at a 37 °C incubator. In the meantime, the 1% Matrigel solution was aspired from the pre-matrigel coated well and replaced with 1 mL fresh mTeSR. After the incubation period, cells were collected with 1-2 mL (depending on the confluency) mTeSR using a 2 mL serological pipette from the hiPSC containing well, homogenized and dissociated by pipetting while being careful not to dissociate

colonies to single cells. Collected cells were then re-plated to the Matrigel coated mTeSR containing wells as a drop (volume of a drop is 5-10 µL), and the plate incubated at 37 °C, 5% CO_2.

3.6.1.2. Differentiation of hiPSCs into Multi Zonal Ocular Cells

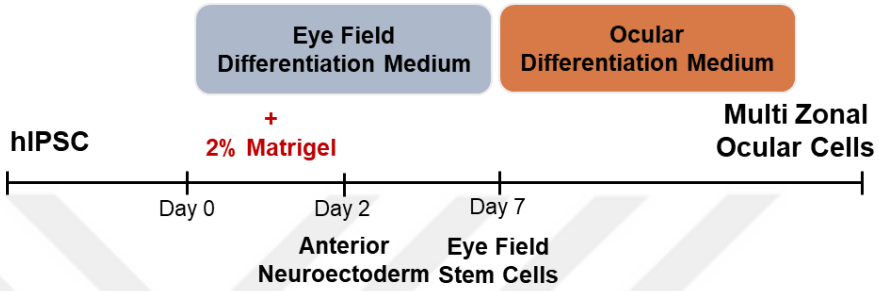

Figure 11. Ocular differentiation of human induced pluripotent stem cells protocol

WT1 hiPSCs were differentiated to multizonal ocular cells by adapting the published protocol of Li et al (Li et al., 2019). By this protocol, hiPSCs were differentiated firstly into anterior neuroectoderm cells by day 2 and eye field stem cells at 7 days, then they differentiated and maturated into multi-zonal ocular cells in approximately 21 days (Figure 11). Eye field differentiation medium (EDM) consisted of DMEM/F-12 and neurobasal medium (Gibco, 21103049) in a 1:1 (v:v) ratio, supplemented with 2 mM L-Glutamine (Gibco, 25030081) 0.1 mM non-essential amino acids (NEAA; Lonza BioWhittaker, 13-114E), 0.1 mM Monothioglycerol (MTG; FUJIFILM Wako Pure Chemical Corporation), 1% N2 Max (R&D Systems, AAR009). Ocular differentiation medium (ODM) was included DMEM/F-12 supplemented with 10% knockout serum replacement (Gibco,10828-028), 2 mM L-Glutamax, 0.1 mM NEAA and 0.1 mM MTG.

Prior to cell seeding, experiment plates were coated with 1% Matrigel as described in section **3.6.1.1.** 1-week cultured hiPSCs were examined under the microscope, differentiated cells were labeled and removed from the culture. The remaining colonies were washed with ice-cold DMEM/F-12. Cold medium helps to dissolve the Matrigel. 1 mL of ReLeSR was added and incubated at room temperature

for 1 min. After aspiration of the ReLeSR, the empty plate was incubated at 37 °C incubator for 4 min. Colonies were collected (minding not to disrupt) with 1 mL of mTeSR using a 2 mL serological pipette. A drop of cells seeded onto pre-matrigel coated wells and cultured in 2% Matrigel containing EDM. The next day, the media was changed with fresh 2% Matrigel mixed with EDM, so that the colonies cultured in 2.5D formed with 2% Matrigel medium mixture for 2 days. From that point on, 2% Matrigel was no longer required, and media was changed with fresh EDM for 5 more days. Thereafter, the culture medium was changed to ODM and refreshed every day however one day per week, the culture was double fed (2-3 mL per well of a 6-well culture plate). The culture was expanded as needed (maximum 75 days in this work).

3.6.2. 3D Organoid Modeling

3.6.2.1. 3D Organoid in Microchip Platforms and Culture Plates

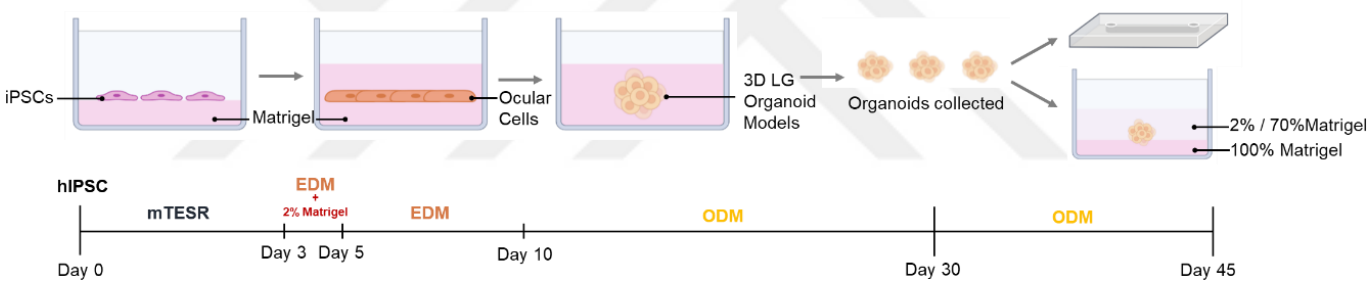

Figure 12. 3D lacrimal gland organoid development protocol

For modeling lacrimal gland organoids from hiPSCs, a new protocol was created (Figure 12). To generate LG organoids *in vitro*, Matrigel coated sterile flat bottom 96-well culture plates were used. First, some wells were coated with 1% while remaining wells were coated with basement membrane Matrigel (Corning, 354234) at 100%. The coating was performed on ice, 100% Matrigel coated plates were coated about half an hour before cell seeding and incubated at 37 °C incubator. Longer incubation times may dry the Matrigel, thereby incubation was not exceeded half an hour.

hiPSCs were collected as described in section **3.6.1.1.** with 1 mL mTESR, homogenize by pipetting without disturbing colonies, and 5 µL of cell solution (200:1; v:v) were seeded on coated plates. Cells were cultured in mTESR for 3 days, the differentiation medium was administrated afterwards. For the next 2 days, EDM

containing 2% Matrigel was given, and refreshed in each day. The culture was continued with EDM (without Matrigel) for 5 more days. On day 10, the differentiation medium was changed to ODM and refreshed every day. On day 30, after the media was aspirated, organoids were washed with cold PBS. Cold PBS helps to remove Matrigel, as well as clean the organoids from unwanted particles and dead cells. Organoid models were then collected using a lancet and passaged to either microfluidic platforms or 96-well plates to grow individually.

Microfluidic platforms were made of polymethyl methacrylate (PMMA) and contains 1 inlet opening for the fresh media input and 1 outlet opening for dirty media output. The area & volume of the microchips were equal to the 96 well plate wells. Media was given by a flow for creating a dynamic culture condition. The flow was controlled by a syringe pump, given at a rate of 0.5 µL/min. Like culture plates, microchips were coated with 100% Matrigel and incubated at 37 °C for half an hour before cell seeding.

Collected organoids were placed in either microchips or cell culture plate, ODM containing 2% Matrigel or 70% Matrigel was given on top. In the next days, ODM without Matrigel was given. Media was refreshed every day in static culture conditions. The flow was given for 1 week. While some microchips were on flow, some stayed as static as a control group, and their media were refreshed every day. At the same time as dynamic culture, static culture (plate and control microchips) was continued.

3.6.3. Lacrimal Gland on Chip

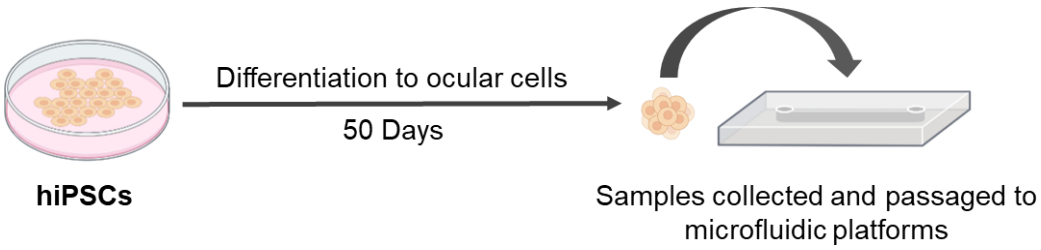

Figure 13. hiPSCs derived ocular cell culture in dynamic conditions

hiPSCs were differentiated into ocular cells as described in section **3.6.1.2.** Culture continued for 50 days, after maturation, cells transferred into microfluidic platforms (Figure 13). Microfluidic platforms that are made up of PMMA were coated with 1% Matrigel. Chips

were designed in the same way as in **3.6.2.1.**, however this time the volume of the chips was equivalent to one well of the 48-well plate due to the size of the samples. Matrigel coating was performed as described in section **3.6.1.1.** at least an hour before the passaged and incubated at 37 °C in the incubator until cell seeding. Media aspirated from the culture plate and cells washed with PBS. Maturated samples were observed under the microscope, selected by their morphologies, collected mechanically using a lancet, and passaged to pre-coated microfluidic platforms. Microchips were incubated at 37 °C, 5% CO_2, some were cultured under dynamic conditions and others stayed as static cultures. The flow was started after 3 days from the passage and was provided at a rate of 0.5 µL/min by syringe pump. Microchip cultures were continued for 1 week.

3.6.4. Stimulation of Budding and Branching Morphogenesis on 2.5 D Culture Condition

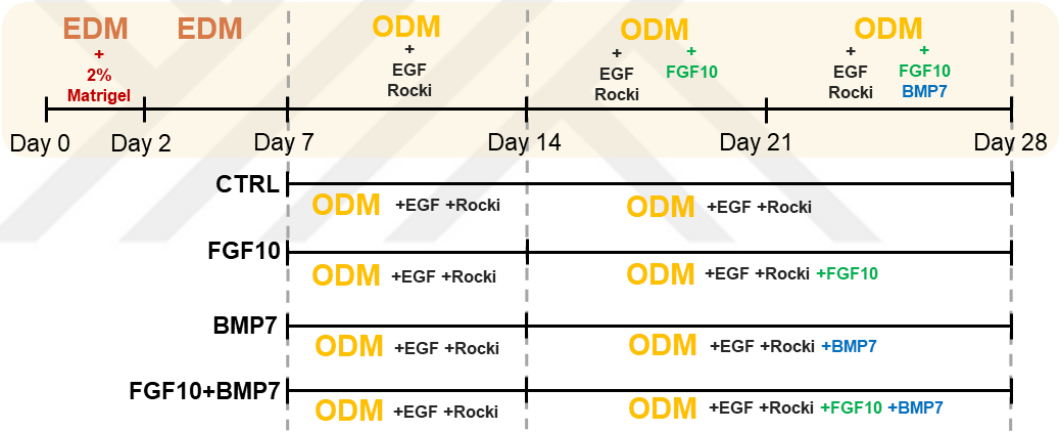

Figure 14. Lacrimal gland branching morphogenesis stimulation protocol

To induce budding & branching morphogenesis, the differentiation of hiPSCs to ocular cells was adapted by the addition of 10 ng/µL EGF, 10 µM, Rocki (Y-27632), 80 ng/µL FGF10 (Biolegend, 559304), and 60 ng/µL BMP7 (Biolegend, 595602) at different time points to the culture medium (Figure 14). The concentration of the supplementary molecules was decided according to literature (Xiao & Zhang, 2020). In this experiment, 1% Matrigel coated 24-well sterile culture plates were used, coating was performed similarly as in section **3.6.1.1.** hiPSCs were seeded at a density of 1000 cells/well. The culture medium refreshed every day.

For the first 7 days, the protocol described in **3.6.1.2** was employed to differentiate iPSCs into eye field stem cells. After 1 week of culture in EDM, the medium was changed to ODM containing 10 ng/µL EGF and 10 µM Rocki for the next 7 days. Four different treatment mediums were given to the cultured cells. The control group was cultured in the same media throughout the experiment. On day 14, 80 ng/µL FGF10 was added to the culture medium of the second and fourth groups. Cells cultured with ODM supplemented with FGF10 medium for the next 2 weeks. 60 ng/µL BMP7 was added to the mediums on the last week of the experiment, given to the only BMP7 containing group and the FGF10+BMP7 containing group.

3.6.4.1. Stimulation of the Branching Morphogenesis of Lacrimal Gland Organoids

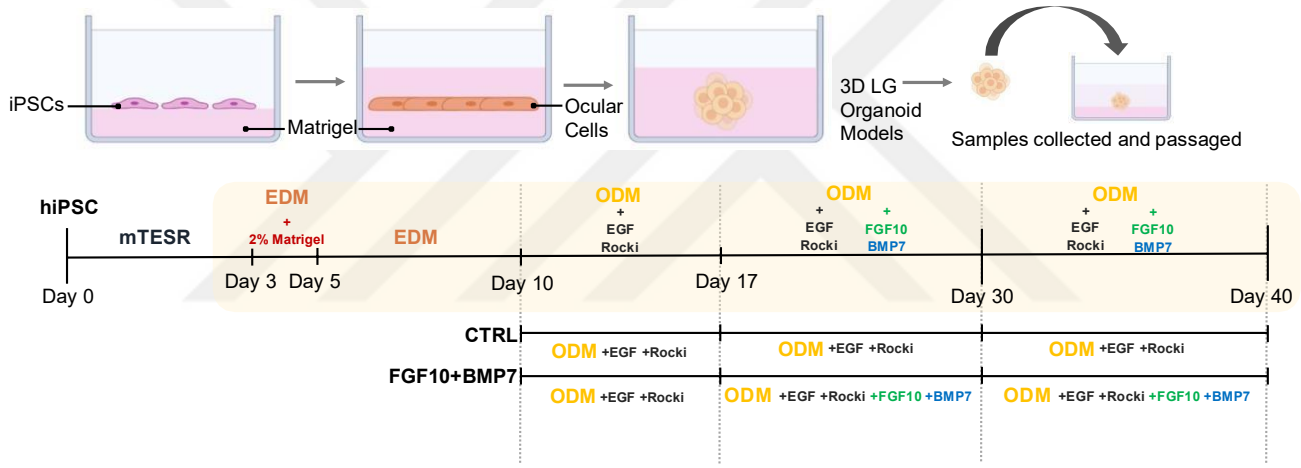

Figure 15. Lacrimal gland branching morphogenesis stimulation of 3D organoids protocol

Organoid models were constructed as explained in section **3.6.2.1.** from hiPSCs, early differentiation to ocular cells was stimulated by EDM for 7 days, supported with 2 % Matrigel on the first 2 days. On day 10, cells were cultured with ODM including EGF and Rocki, the same concentrations used in section **3.6.4.** for 1 week. After 7 days, additional supplements FGF10 and BMP7 were added to the medium of one group of cells while the remaining cells stayed in ODM+EGF+Rocki medium as control (Figure 15). Mediums were refreshed every day**.** Organoids were passaged to pre-matrigel coated microfluidic platforms on day 30. The sizes and the volume of the microchips were equal to the 96-well plate wells. Starting on day 33, the flow was given at a rate of 0.5 µL/min for 1 week. Mediums were the same as the plate culture.

3.6.5. Cell Characterization

Differentiated cells were characterized by their gene expressions and protein expression levels. Here, quantitative polymerase chain reaction PCR (qPCR) was used to analyze gene expression. To perform qPCR, samples were prepared by RNA extraction from organoid models/cell culture, complementary DNA (cDNA) synthesis from extracted RNAs, and primers designed for specific genes. Immunofluorescence staining (IF) was used to detect protein expressions. Samples were prepared for IF staining by firstly OCT embedding, then sections were prepared using the cryostat device.

3.6.5.1. RNA Extraction

RNA extraction and purification were performed using Macherey-Nagel RNA isolation kit (740955.50) according to the manufacturer's instructions. Adherent cells were collected from the culture plates and platforms using Trizol reagent (Molecular Research Center, TR 118) after washing with PBS. Cell scraper was used to collect the adherent cells, for $1x10^6$ cells, 1 mL of Trizol was used. The lysates were transferred to Eppendorf tubes and kept at -80 °C until the next step.

After the cell lysates were thawed, samples were homogenized using a homogenizer or by pipetting and incubated at room temperature for 5 minutes. 20% Chloroform was added to samples by the volume of Trizol. Afterward, Eppendorf tubes were gently shaken up and down 20 times and incubated for 2-3 min at room temperature. Following the incubation, samples were centrifuged at a rate of 12.000g for 15 minutes at 4 °C. After the centrifugation, 3 different phases occurred on the samples. The RNA containing the aqueous phase was collected from each sample carefully and transferred into new sterile nuclease-free Eppendorf tubes. 70% Ethanol by the volume of the collected aqueous phase was added and mixed by pipetting. Tubes were incubated at room temperature for 10 min. From that point on, the isolation process proceeds with the MN RNA Isolation kit.

The eluted RNA quantity and purity were measured with the Nanodrop device. Samples were kept at -80 °C until the further step, cDNA synthesis.

3.6.5.2. cDNA Synthesis

ABM OneScript Plus cDNA synthesis kit (G236) was used according to the manufacturer's protocol. RNA samples and other components were thawed on ice. 4 µL 5X RT Buffer, 1 µL dNTP (10mM), 1 µL OneScript Plus RTase and 1 µL Primer (10 µM) were mixed for one 20 µL reaction. RNA concentrations were calculated to be equal at the end of the reaction, Nuclease Free H_2O was added up to 13 µL. Prepared reaction tubes were placed into the thermal cycler machine. The reaction was carried out at 55 °C for 15 min and stopped by cooling at 4 °C. The resulting cDNAs were kept at -20 °C until the next step.

3.6.5.3. Primer Design

NCBI primer design tool was used for primer design. The gene sequences were taken from NCBI Basic Local Alignment Search Tool (BLAST) website. Glyceraldehyde-3-phosphate dehydrogenase (GAPDH) was used as a housekeeping gene in qPCR experiments. Primers were diluted with nuclease-free H_2O to 100 µM and stored at -20 °C until use. Prior to the experiment, primers thawed on ice and adequate amounts were diluted to 10 µM. The sequences of the primers used in this study were given at the belove (Table 1).

Table 1. Primer sequences used in qPCR experiments

Gene	Forward Primer (5'-3')	Reverse Primer (5'-3')	Tm (˚C) (F/R)
AQP5	GAACCCAGCCCGCTCTTTTG	AGTCCTCGTCAGGCTCATACG	62/62
COL1A1	CCGATGTGCTCCACTAACCT	GGCCAAGTTTAGAGCCACAG	59/59
COL9A2	CAGCTTCCTGCACTGTCTGA	GACGAGGGGCACTACATCTC	59/61
FGF10	GAAATCGGAGTTGTTGCCGTC	TGCCACATACATTTGCCTCC	62/58
FGFR2	GATAAATACTTCCAATGCAGAAGTGCT	TGCCCTATATAATTGGAGACCTTACA	60/60
GAPDH	ACCACAGTCCATGCCATCAC	TCCACCCTGTTGCTGTA	59/53
LGR5	GAGGATCTGGTGAGCCCTGAGAA	CATAAGTGATGCTGGAGCTGGAA	62/61
MMP2	CACTCACAGACCTGACTCGGTT	AAGCAGGATCACAGTTGGCTGG	62/62
MMP9	GAACCAATCTCACCGACAGG	GCCACCCGAGTGTAACCATA	59/59
NDST1	ACCAGAGAAAGGCAGAGACC	GTCACTGCACTTTGTCCCTG	59/59
P63	GCAGTCGAGCACCGCCAAGT	TCAAAGCAGCGTCGGCCCAG	60/61
PAX6	CAGAGCCCCATATTCGAGCC	CAAAGACACCACCGAGCTGA	61/59
SOX9	GTACCCGCACTTGCACAAC	TCTCGCTCTCGTTCAGAAGTC	59/60

3.6.5.4. Quantitative Real-Time PCR (RT-qPCR)

Promega GoTaq qPCR Master kit (A6002) was used for the qPCR experiment according to the manufacturer's instructions. Kit components and cDNA samples were thawed on ice prior to use. For statistical calculation, 3 biological and 3 technical replicates were taken for all experimental groups. For each well, 10 µL reaction consisting of 5 µL GoTaq qPCR master mix (2X), 1 µL Forward, 1 µL Reverse Primer (10 µM), 2 µL nuclease-free water, 1 µL cDNA (10 ng/ µL) was prepared. After plating the reaction mixtures, the plate was sealed and centrifuged at 1200 rpm for 5 mins. The reaction setup explained in Table 2, was run using Applied Biosystem 7500 Fast real-time PCR system.

Table 2. qPCR Protocol

Stages	Number of Cycles	Temperature (˚C)	Time (second)
Holding	1	95	120
Cycling	40	95	10
		60	10
		72	30
Melt Curve	1	95	15
		60	60
		95	15
		4	∞

The quantification comparative was chosen as Ct (ΔΔCt). For those who do not calculate by the program, the ΔΔCt values were calculated using Excel.

Calculation done by given formulas: Ct_{sample}-$Ct_{housekeeping\ gene\ avarage}$=ΔCt;

$\Delta Ct_{control\ average}$-$\Delta Ct_{sample}$=ΔΔCt

Fold changes were calculated by $2^{-\Delta\Delta Ct}$ values.

3.6.5.5. Immunofluorescent Staining

Immunofluorescence (IF) staining methods were used to examine the protein expression levels in the cells. Stained cells/organoids were visualized using fluorescence microscopy (Olympus BX61) and confocal microscopy (Zeiss LSM880). Taken images were analyzed using Zeiss and ImageJ programs.

3.6.5.6. Immunocytochemistry Assay (ICC)

Cells to be stained were washed with PBS 3 times after aspiration of the medium from the culture plates. Fixation was performed via incubating cells for 20-30 mins with 4% PFA (Sigma Aldrich) at room temperature. After the incubation, the PFA solution was aspirated, and cells were washed with PBS 3 times. The fixated sample was incubated with fresh PBS at 4 °C until further processes or directly placed in a freshly prepared 30% sucrose solution and was incubated at 4 °C until the sample sank to the bottom of the tube/well.

Once the sample sank, it was transferred in Optimal Cutting Temperature (OCT; Sakura; 4583) and was snap frozen by placing in liquid nitrogen upon embedding. Samples embedded in OCT were stored at -80 °C until cryosectioning. 7µm sections were cut by the cryostat device and sections were placed on polylysine microscope slides (Thermo-scientific). Slides were kept at -80 °C until the staining step.

All buffers were warmed at room temperature before starting the experiment. Slides were thawed at room temperature for 20 min prior to staining. The samples were labeled and surrounded with a Pap pen. Permeabilization was performed by incubating the samples in the permeabilization buffer containing 0.3% Triton X-100 in PBS (v/v) for 15 mins at room temperature. The samples were washed with 0.05% Tween20 containing PBS (PBS-T) 3 times for 5 minutes. After the PBS-T solution was removed from the slides, the blocking buffer consisting of 1% Bovine Serum Albumin (BSA) in PBS-T (w/v) was added to perform blocking. The samples were incubated at room temperature for 1 hour with blocking buffer, then washed with PBS-T 3 times for 5 times. Primary antibodies diluted with antibody dilution buffer (1% BSA + 0.3% Triton

X-100 in PBS) according to the given table (Table 3). Diluted antibodies were given to the samples, and the slides were incubated at 4 °C overnight. After the incubation, the antibody solution was removed, and the samples were washed with PBS-T 3 times for 5 min. Secondary antibodies were diluted with antibody dilution buffer as described in the Table 3 as well. Diluted secondary antibodies were added to the samples and the slides were incubated at room temperature for 2 hours protected from light. Following the incubation, slides were washed with PBS 3 times for 5 min. Lastly, DAPI diluted to 1 µg/mL with PBS was added to samples and incubated in the dark for 10 minutes at room temperature. After washing slides with PBS 3 times for 5 min, a mounting medium was added, and slides were covered with coverslips. Slides were stored at 4 °C until visualization with fluorescence/confocal microscopy.

Table 3. Antibody List

Antibody	Brand & Cat. No.	Host	Dilution
Primary Antibodies			
Anti-Lactoferrin	Abcam, ab109216	Rabbit	1:200
Anti-Lipocallin-2	Abcam, ab41105	Rabbit	1:25
Anti-α Smooth Muscle Actin	Cell Signaling, 48938S	Mouse	1:200
Aquaporin 5	Bioss, bs-1554R	Rabbit	1:200
Cytokeratin 5	Thermo, MA517057	Mouse	1:200
Cytokeratin 19	Cell Signaling, 4558	Mouse	1:200
E-Cadherin	Bioss, bs-10009R	Rabbit	1:200
Ki-67	Bioss, bs-2130R	Rabbit	1:200
LGR5	Novus, NBP1-28904SS	Rabbit	1:1000
PAX6	Novus, NBP2-44576	Mouse	1:200
Phospo-β-Catenin	Cell Signaling, 4176	Rabbit	1:100
Secondary Antibodies			
Anti-Mouse	Jackson Immuno 715-585-150	Donkey	1:800
Anti-Rabbit	Jackson Immuno 715-545-152	Donkey	1:800

3.6.5.7. Whole Mount Staining

Organoids to be stained were washed with cold PBS 3 times after aspiration of the medium from the culture plates. To those who embedded in Matrigel, centrifugation (1600 rpm 5 min) was used in the last washing step, and organoids were then transferred into sterile 96-well culture plates. Fixation was performed via incubating

cells for 1 hour with 4% PFA at room temperature. After the incubation, the PFA solution was aspirated, and cells were washed with PBS 3 times.

All buffers were warmed at room temperature before starting the experiment. Permeabilization was performed by incubating the samples in the permeabilization buffer for 30 min at room temperature on a shaker at approximately 40 rpm. The samples were then washed with PBS-T 3 times for 5 min. After the PBS-T solution was removed from the well, the blocking buffer was added to perform blocking. The samples were incubated at room temperature for 2 hours with blocking buffer on the shaker, then washed with PBS-T 3 times for 5 times. Primary antibodies were diluted with antibody dilution buffer according to the given table (Table 3). Diluted antibodies were given to the samples and incubated at 4 °C overnight. After the incubation, the antibody solution was removed, and the samples were washed with PBS-T 3 times for 5 min. Secondary antibodies were diluted with antibody dilution buffer as described in the Table 3 as well. Diluted secondary antibodies were added to the samples and incubated at room temperature on a shaker for 2 hours protected from light. Following the incubation, samples were washed with PBS 3 times for 5 min. Lastly, DAPI diluted to 1 µg/mL with PBS was added to samples and incubated in dark for 10 minutes at room temperature. After washing the samples with PBS 3 times for 5 min, organoid samples were placed on microscope slides. The mounting medium was added, and slides were covered with coverslips, colorless nail polish was used to draw around the organoid samples so that the coverslips do not squash the samples. Slides were stored at 4 °C until visualization with fluorescence/confocal microscopy.

3.6.5.8. NAG Assay

N-Acetylglucosaminidase (beta-NAG) Activity Assay Kit (Colorimetric; ab204705) was used to test samples NAG enzymatic activity, thereby the secretion functionality according to the manufacturer's instructions. Fresh standard solutions were prepared by diluting the provided 20mM *p*-Nitrophenol (*p*NP) with NAG assay buffer to 2 mM. All buffers and solutions were used at room temperature after the collection of samples. The assay was performed by either collecting the cells or the mediums, using a 96-well plate. Results were measured at OD 400nm on a microplate reader.

For cell samples, the cells were washed with cold PBS and harvested using a cell

scraper into an Eppendorf tube. Cells were resuspended in 100-200 µL of ice-cold NAG assay buffer and homogenized quickly by pipetting up and down a few times. Samples were centrifuged at 10.000g for 3 min at 4 °C to remove any insoluble material. The supernatant was collected from each sample and transferred into a clean tube. Collected samples can be used directly, otherwise, samples were snap freeze in liquid nitrogen upon extraction and stored at -80 °C immediately. Samples were thawed on ice before using.

Medium samples were tested directly by adding samples to the microplate wells or were snap freeze in liquid nitrogen and stored at -80 °C immediately.

Standard dilutions were distributed as 125 µL to the standard wells, and 2 replicates were performed. Sample wells contained 70 µL, if less, the volume was equilibrated to 70 µL/well with NAG assay buffer. Positive control wells were prepared as 2 replicates, 3 µL of NAG positive control was mixed with 67 µL NAG assay buffer for each well. Sample background control wells were prepared as 70 µL in case the medium samples have different colors. 55 µL of NAG substrate was added into each sample and positive control wells. 55 µL of NAG assay buffer to sample background control wells. The plate was then incubated at 37 °C for 30 min. After incubation, 25 µL of NAG stop solution to all wells. Wells were mixed by pipetting and the plate was incubated at 37 °C for 10 minutes protecting from light. Afterward, the output was analyzed at 400 nm using a plate reader (Thermo, MultiSkan).

3.6.5.9. Sample Preparation for Metabolomics Analysis

Cells of the branching experiment were collected at day 28. First, the media was removed, and washed with 3 mL of isotonic sodium chloride (NaCl) solution. Then, 1 mL of methanol:water (9:1, v/v) solution was added to the cells, and the immediately frozen by placing in liquid nitrogen. After freezing, cells were collected by scraping and transferred into 2 mL Eppendorf tubes. Following the collection, Eppendorf tubes were centrifuged at 15.000 rpm to precipitate proteins. Supernatants were collected after centrifugation and transferred into a new sterile 2 mL Eppendorf tube. Samples were stored at -80 °C until further steps.

Samples thawed at room temperature and evaporated to complete dryness using a vacuum centrifuge (Savant ISS110 SpeedVac Concentrator Thermo Scientific). After that, prepared to GC-MS with necessary chemicals.

3.7. Research Plan

Table 4. Research Plan

Research Plan	September 2020-September 2021	October 2020-December 2021	June 2021-April 2022	May 2022-June 2022
Literature Review	X	X	X	X
Experiment Planning		X	X	
Data Collection and Experimenting			X	X
Evaluation of Data			X	X
Thesis Writing				X

3.8. Evaluation of Data

The Graphpad Prism 8 program and Microsoft Excel were used to analyze qPCR results. Image J and Zen 3.1. programs were used to analyze IF stainings and fluorescence intensity. Metabolomics analyses were carried out by metaboanalyst 5.0.

3.9. Limitation of Research

Variations in hiPSCs collected from different sources and produced via different methods are a common drawback of hiPSC-related investigations. Since we used only one type of hiPSC, the results were different reported in the literature with similar approaches.

After the induction of the differentiation protocol, heterogeneity was the biggest problem. Even after the induction of supporting molecules for specification of the differentiation, the resulting culture was still highly heterogenic, and 3D samples did not show similarity at a high rate. So that, a small amount of them were used for further analyses. Moreover, 3D samples were so small that RNA collection was could not achieved in appropriate concentrations, thereby IF analyzes to test expression levels in protein levels was preferred.

3.10. Ethics Approval

This study was approved by the Non-Invasive Research Ethical Committee of IBG with the protocol number 2021-021 on 26.07.2020. The thesis approval is presented in section 8.1.

4. RESULTS

4.1. Formation of ocular cells from hiPSCs

Wild-type hiPSCs were differentiated into the ocular cells as explained in **Section 3.6.1.2.** Following the cell seeding, differentiation of hiPSCs colonies was started by given stimulatory factors. It was observed under the microscope by their changing morphologies as well as the spreading of cells to surroundings. By day 25, the formation of multi-zones was seen in culture plates. Heterogeneity of the differentiated

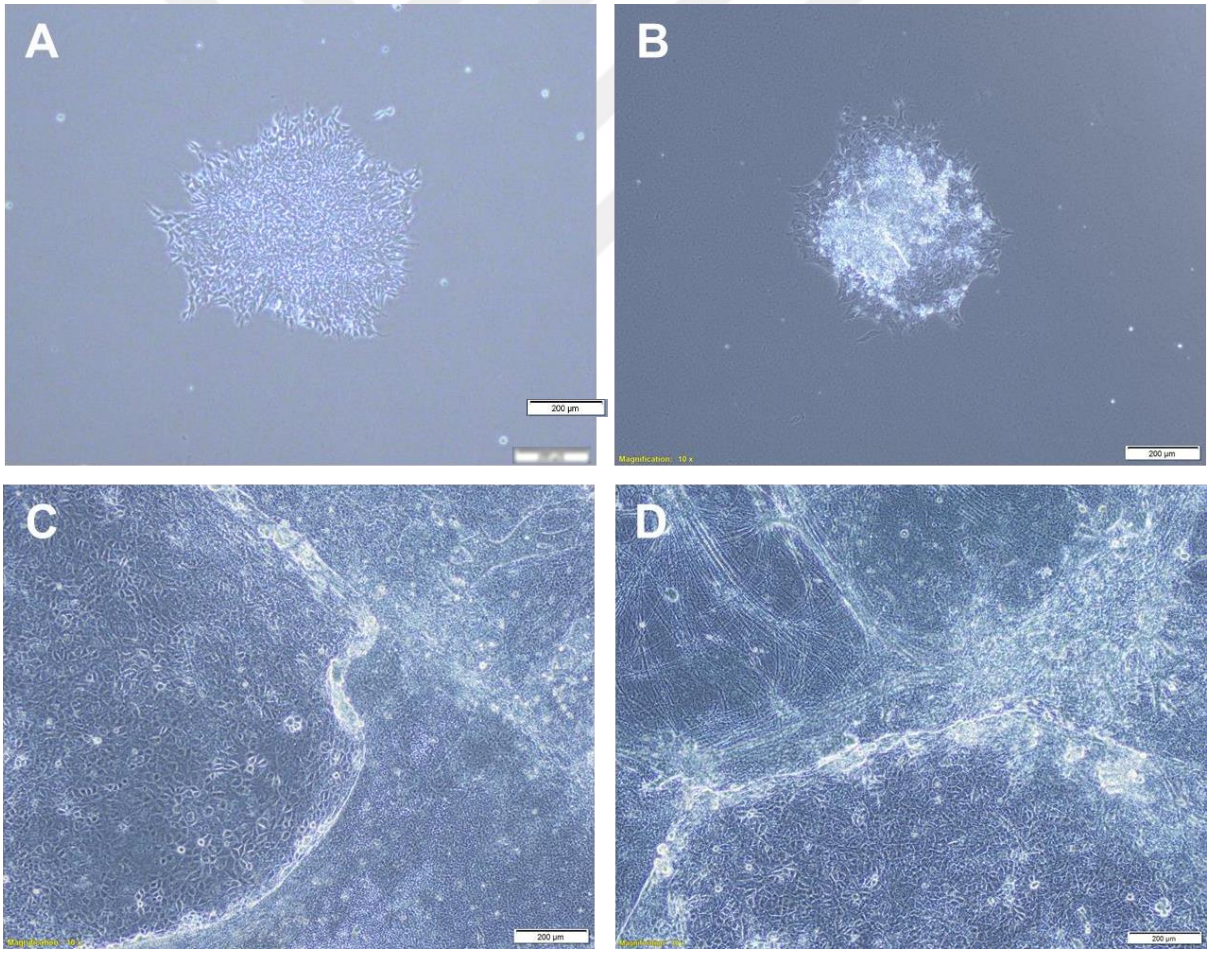

Figure 16. Differentiation of hiPSCs to ocular cells *in vitro*
BF images of A) hiPSC colony on day 3 of iPSC culture, B) Early differentiation on day 7 of the experimental culture, C) Multi-zone formation on day 28, D) Differentiated cells on day 32. Magnification: 10X, Scale bar: 200 µm

cells was quite high; therefore, zones were observed under the microscope (Figure16).

Starting from day 21, the expression of ocular surface ectoderm (OSE) markers such as PAX6 and P63 was expected to increase according to the protocol. In order to analyze the mRNA expression levels, cells were collected and RNAs were isolated. The qPCR results showed that the expression of PAX6 and P63 was significantly increased in the differentiated cells as well as FGF10 compared to the iPSCs, indicating that the differentiation to ocular cells has been successfully applied (Figure17).

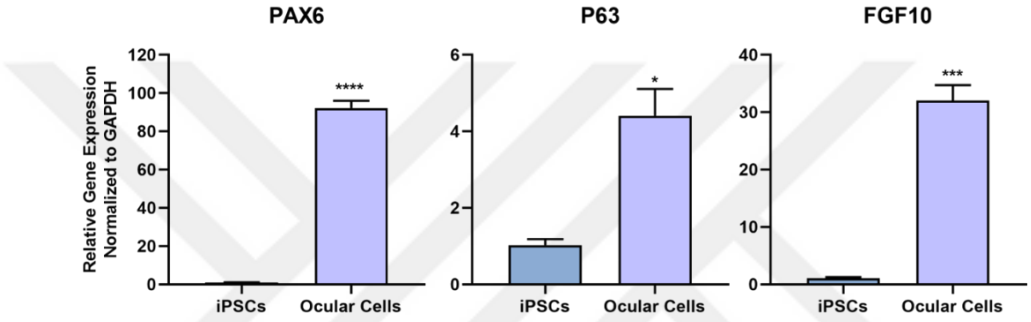

Figure 17. mRNA expression levels of ocular genes compared to hiPSCs

PAX6, P63 and FGF10 mRNA expression levels in hiPSCs and differentiated ocular cells on 21 days. p<0.00005: ****, p<0.0005: ***, p<0.005: **, p<0.5: *

Further analysis was performed via IF staining to examine the protein expressions. Since not much is known about the role of LGR5, the expression levels were investigated together with PAX6. Interestingly, LGR5 protein expression was seen more on the edges of the cryosections (Figure 18A). Moreover, our preliminary data has been shown that the expression of LG-related genes was significantly high even during long culture periods (Melis Asal, 2020). In light of these preliminary data, LGR expression was investigated during different time periods (at day 7, 14, 21, 35, and 45) to analyze the changes of the longer-term culture periods. Change in the expression level of LGR5 was not found as specific to culture time, it peaked around day 14 and was suddenly lowered one week after. Following that, it had a peak again at 35th days and was decreasing at 45 days (Figure 18 B).

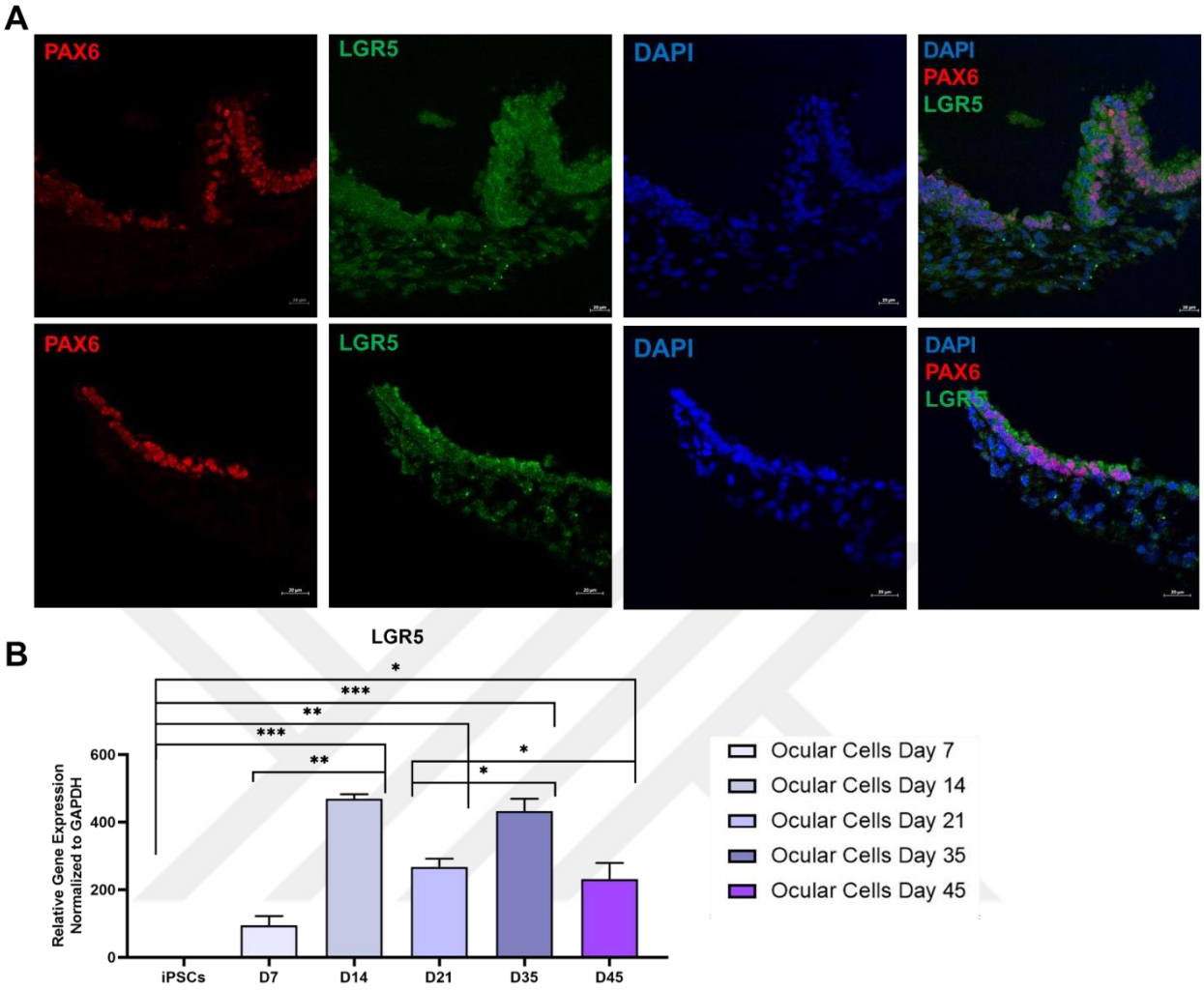

Figure 18. LGR5 expression in ocular cells differentiated from iPSCs
A) IF images of 35 days old LG-like structure cryosection stained with LGR5 (green) and PAX6 (red) antibodies. Nuclei staining was performed via DAPI. Scale bar: 20 μm. B) mRNA expression level of LGR5 in samples from different time periods.

Moreover, since LGR5 expression was found at mRNA and protein levels in the differentiated samples, further analyze was performed on examining the expression of WNT β-Catenin at the protein level. Sections from 45 days and 70 days old multi-zonal ocular cells were stained against phospho-β-Catenin and nuclei with DAPI. Results were suggesting that the β-Catenin expression was observed mostly in ductal cells and at the periphery similar to LGR5 (Figure 19).

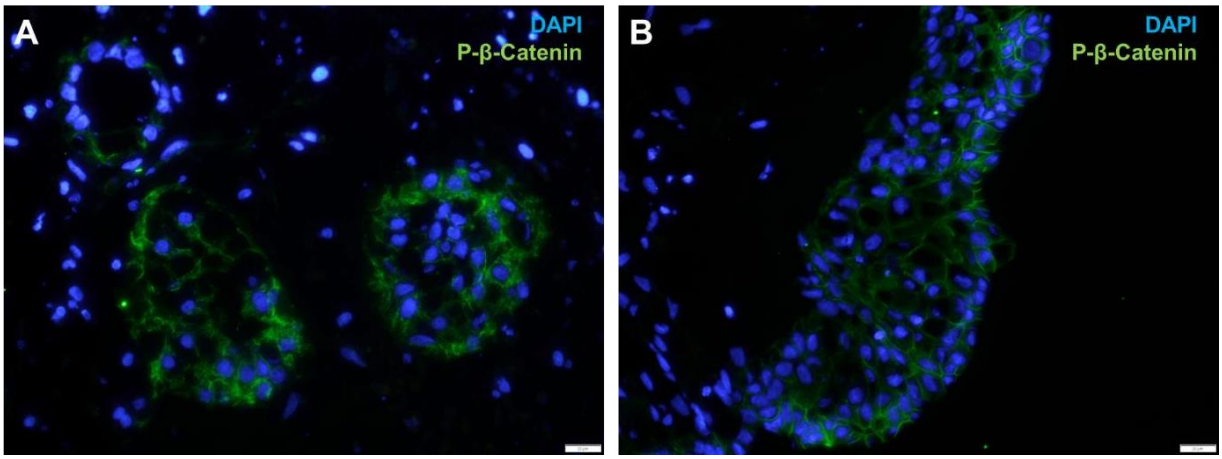

Figure 19. Phospho-β-Catenin staining in ocular cell samples
IF imaging of Phospho-β-Catenin (green) staining A) on day 45 and B) on day 70. Nuclei stained with DAPI. Scale bar: 50 µm.

When iPSCs were differentiated into multi-zonal ocular cells, some formed LG-like structures (Figure 20). These structures resemble the branched morphology of the LG with ducts. For the most part, these structures appeared after around 30 days. Analysis of LG-related gene expression levels including secretion marker LYZ, LTF acinar marker AQP5, or mucin marker M5AC has been reported in earlier studies (Melis Asal, 2020). The data was promising as it showed a characteristic similar to the human LG. However, the rate of the formation and efficiency of LG-like structures in this heterogenic culture was extremely low. Thereby, a more efficient protocol was needed.

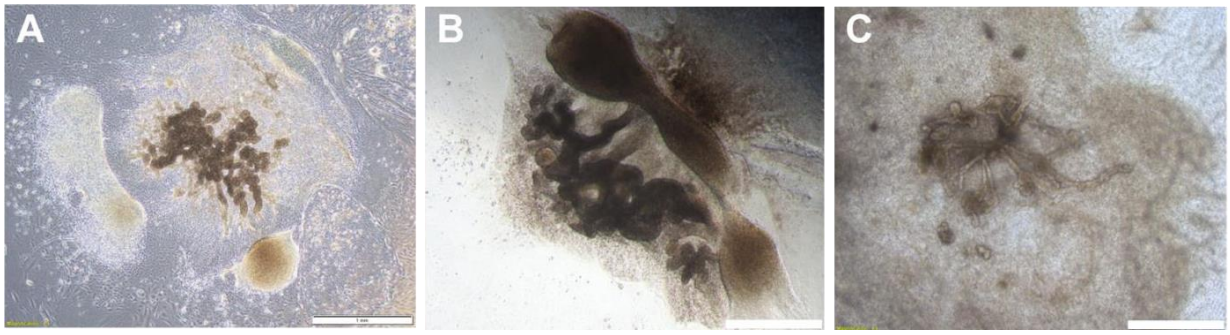

Figure 20. LG morphology in differentiated hiPSC culture
BF images of observed LG morphology on A-B) Day 35, C) Day 38. Magnification: 4X, Scale bar: 1 mm.

4.2. Lacrimal gland organoid models derived from hiPSCs

To induce organoid formation, hiPSCs were seeded on either 1% or 100% Matrigel coated well plates. 1% Matrigel coated groups did not support 3D organoid formation, thereby experiments were run with 100% Matrigel coating from that point on. Differentiation factors were given after 3 days. The scenario where the differentiation process was started on the day where cells seeded also was tried, however, the cells died in a short period of time in this case. Thereby, cells were adapted to the new culture condition in 3 days without differentiating. On the first day of culture, colonies were in round shape (Figure 21A). The organoid-like structure was observed starting approximately on day 8 under given conditions. The organoid culture was extended for 1 month. Maturated organoid models were then collected and passaged to either microfluidic platforms or 96-well plates to grow individually. Some organoids were fixated, while some of them are passaged, IF staining was performed for those who have fixated for ductal and myoepithelial cell markers. Organoids showed AQP5 and LCN expression, indicating the presence of acinar cells, as well as CK5 and CK19, indicating the presence of myoepithelial cells (Figure 22). The expression of both acinar and myoepithelial cell markers suggests that iPSCs are differentiated into lacrimal gland organoids.

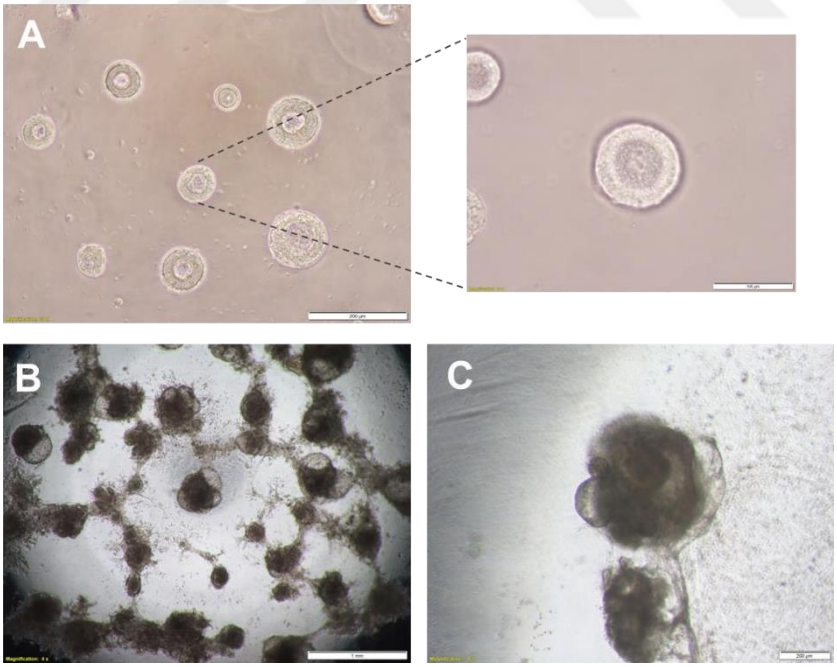

Figure 21. hiPSC derived organoid models

BF images of organoids showing A) First day of the organoid culture in different magnifications. Scale bars: 200 µm, 100 µm respectively. B) Growing organoids on day 8. Scale bar: 1mm. C) Day 16. Scale bar: 200 µm.

For organoids which were passaged to microfluidic platforms and were cultured under dynamic conditions, the flow was started 3 days after the passage and given for 2 weeks. However, the flow time was so long that organoids started to die. For that reason, the flow was shortened to 1 week.

Most of the organoids that are embedded with 2% Matrigel after passaging were not proliferate enough and died eventually, thereby 70% Matrigel coating was selected as the top coating. Passaged organoids to the 96-well plates continued to grow and some created brachial structures while some showed swelling structures (Figure 23).

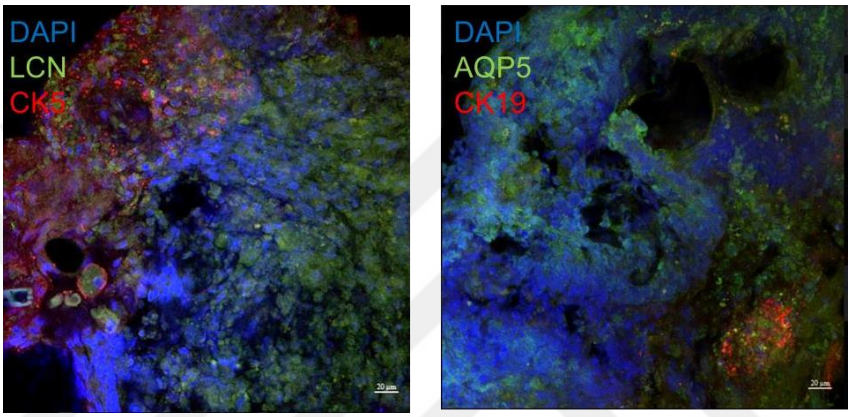

Figure 22. Ductal and myoepithelial protein expression in 1-month old organoids
Samples stained with acinar cell markers LCN and AQP 5 (green), myoepithelial cell marker CK5 (Red), and ductal marker CK19 (red). Scale bar: 20 μm.

For those passaged organoids to the microfluidic platforms, dynamic conditions showed better results compared to the static conditions (Figure 24). Almost all of them were attached to the surface. Branchial structure formation was observed in many of the dynamic platforms, as well as swelling structures. On the other hand, those who were grown under static conditions shrunken compared to the first passaged sizes and showed almost no branchial structures.

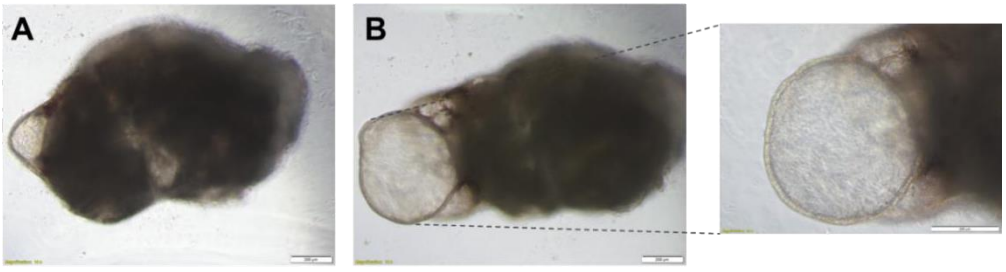

Figure 23. Passaged organoid showing swelling structure
Passaged organoids to microfluidic chips grow under either dynamic or static culture conditions BF images of LG organoid passaged and embedded to Matrigel within microfluidic platform on A) day 1 and B) day 8. Scale bars: 200 μm.

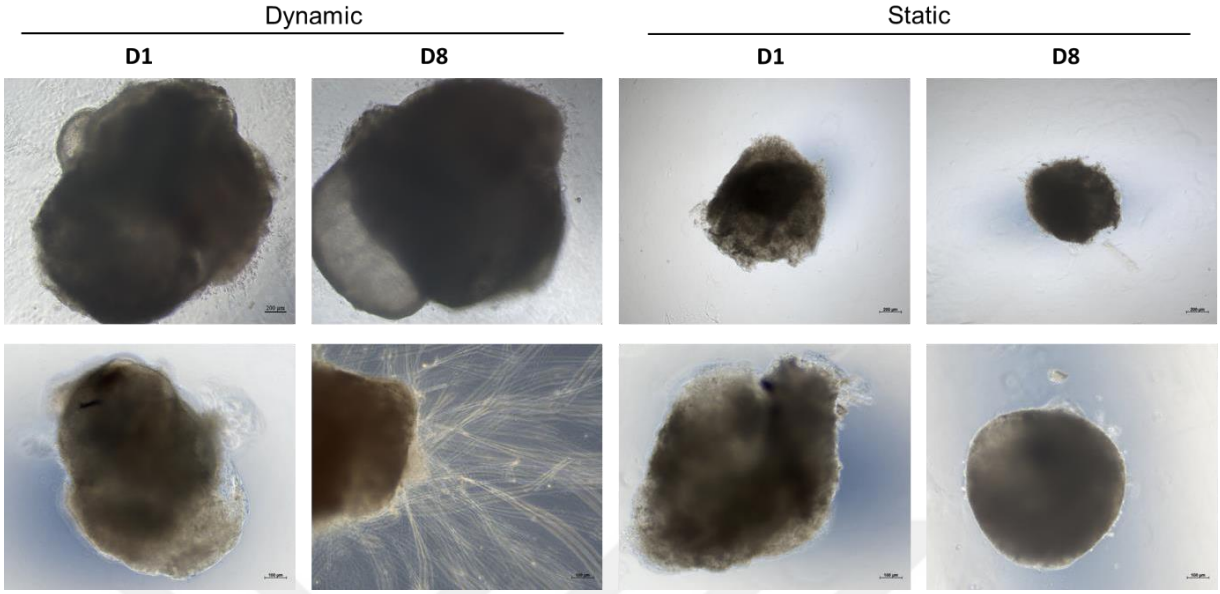

Figure 24. Passaged organoids to microfluidic chips grow under either dynamic or static culture conditions
BF images of passaged organoids and embedded to Matrigel in microfluidic platforms on day 1 and day 8. Scale bars: 200 μm.

IF stainings of 3D cultured models showed α-SMA expression indicating the expression and localization of MECs. Its expression was found on the edges of the organoids cultured under static conditions, whereas in that are culture under dynamic conditions, its expression was localized interiors of the organoid. On the other hand, LTF expression was relatively low in the samples (Figure 25). However, its expression was better detected in organoids that are grown in static culture conditions (Figure 34).

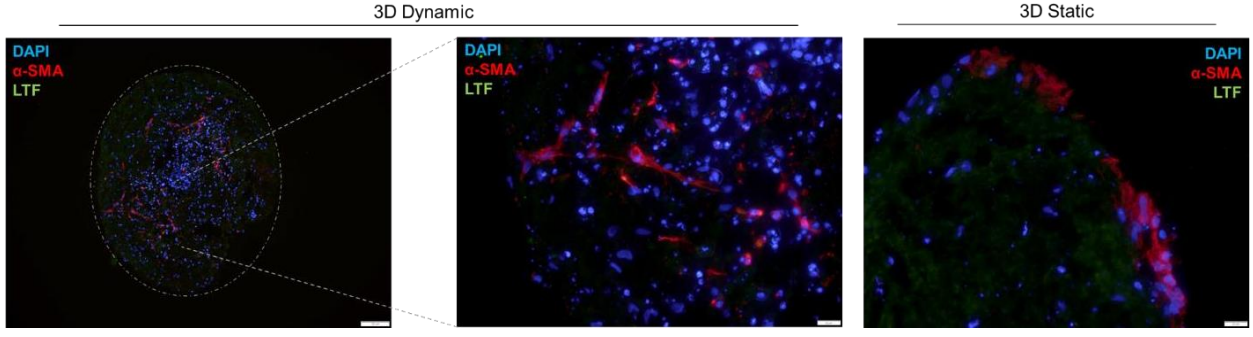

Figure 25. Myoepithelial and ductal marker expression of 3D models
Cryosections of organoids grown under static and dynamic culture conditions stained against myoepithelial cell marker α-SMA and ductal cell marker LTF. Nuclei stained with DAPI. Scale bars: 100 μm and 20 μm respectively.

4.3. Maturated ocular cells continue to grow after passaging to microfluidic platforms

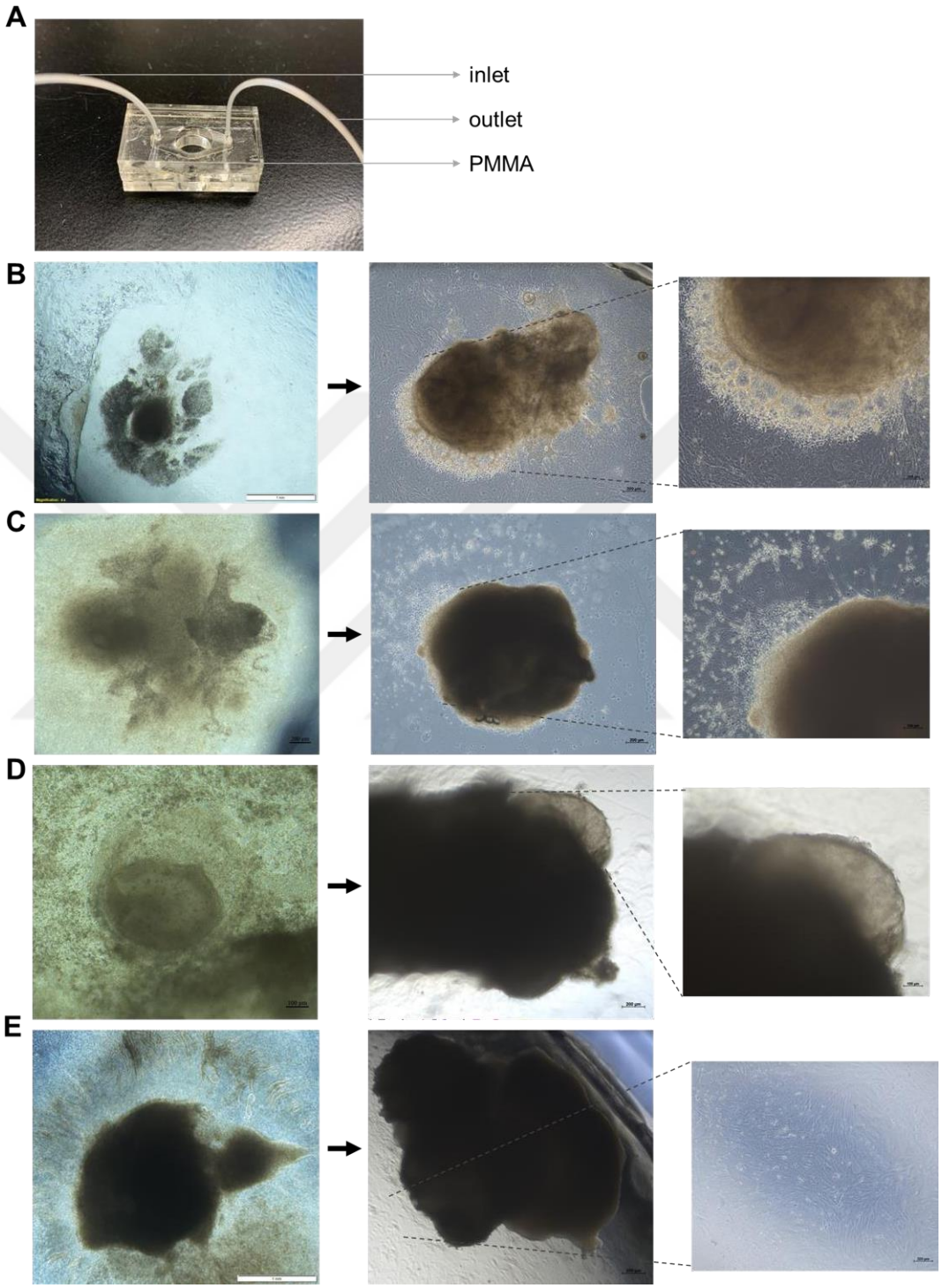

Figure 26. Maturated ocular cells passaged to the microfluidic platforms
BF images of samples. Left column shows 50 days old ocular cell culture differentiated from iPSCs. Right columns show 10 days after the passage to the microfluidic chips. A) Microfluidic chip. B and C) Growth under dynamic culture conditions. D and E) Growth under static conditions.

Ocular cells differentiated from hiPSCs were maturated for 50 days under culture conditions. Thereafter, samples were collected and passaged to microfluidic platforms to grow under either static or dynamic culture conditions. Unlike the organoids that are passaged for 30 days (results section 4.2.), all these samples were alive, they proliferate and continued to grow in microfluidic platforms while forming branchial structures and swelling structures (Figure 26). If static conditions were compared with dynamic conditions, the samples grown under flow were better at branching and proliferating according to their morphologies. Nevertheless, in both conditions but mostly under static conditions, cells attached to the surface proliferate, which means the conditions are proper for cell growth (Figure 26D).

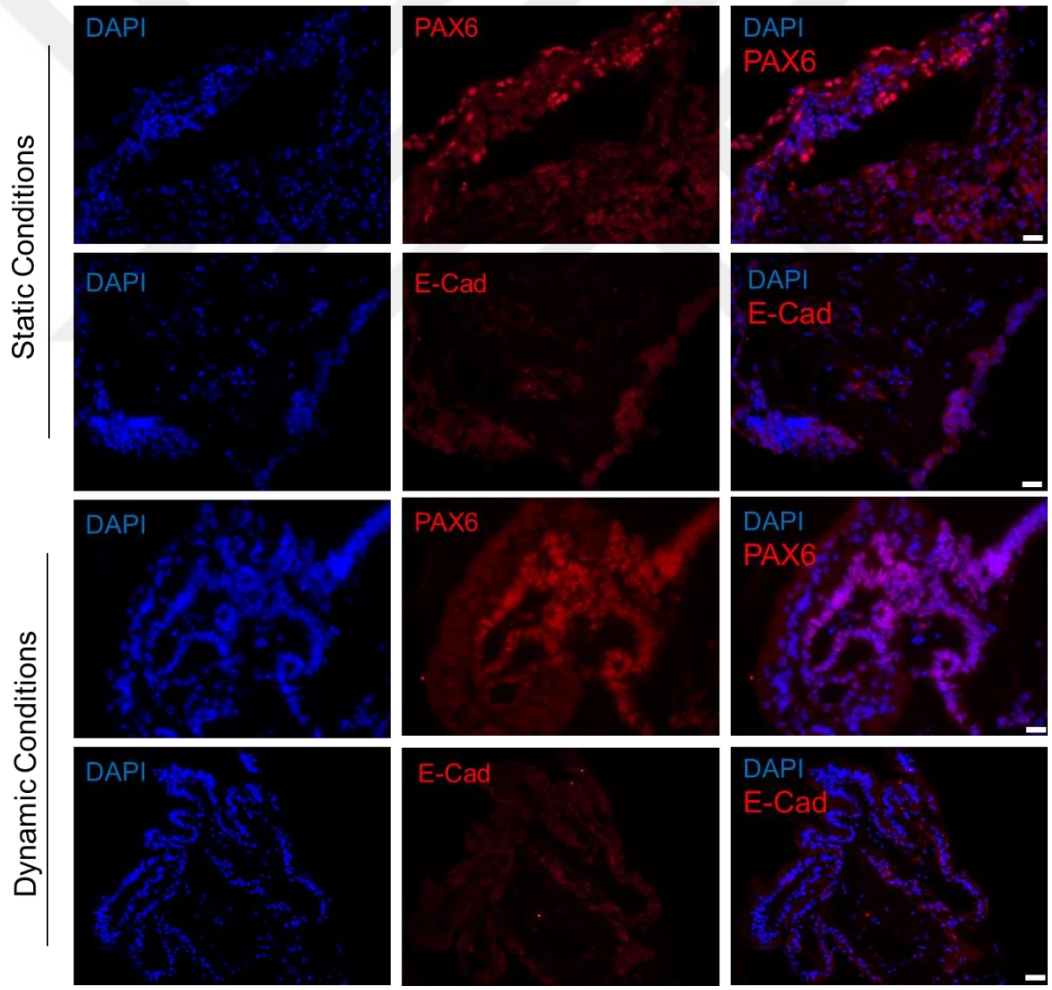

Figure 27. Protein expression levels of organoids grown under static and dynamic culture conditions.
Samples stained against PAX6 and E-Cadherin (red). Nuclei stained with DAPI. Scale bar: 20 µm.

To observe the ocular cell differentiation at the protein level, sections were stained against PAX6, and for cell adhesion, they were stained with E-Cadherin. For most of the samples, PAX6 expression was present in the nuclei of the cells, indicating the samples have successfully differentiated into ocular cells (Figure 27). Besides, lactoferrin expression was also found in the samples, indicating that they exhibited lacrimal gland features (Figure 28).

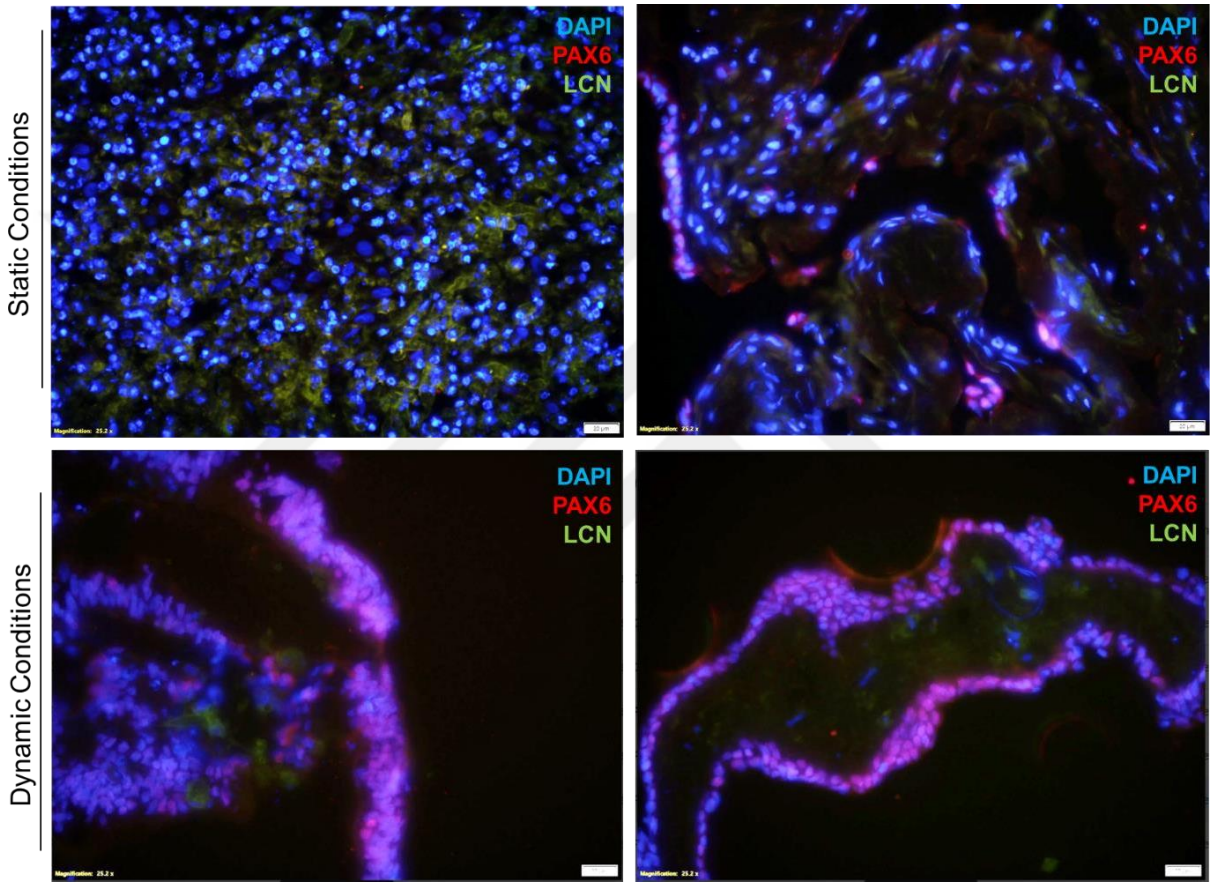

Figure 28. Ocular differentiation marker and ductal cell marker staining of organoids grown under static and dynamic culture conditions
LG on chip samples was stained against PAX6 (red) and LCN (green). Nuclei stained with DAPI Scale bar: 20 μm.

4.4. LG branching morphogenesis induction via FGF10 and BMP7

Stimulatory factors were given to organoid models to better mimic branching morphogenesis. FGF10 and BMP7, as the main initiator factors of budding and branching of the epithelium through the mesenchyme, were given to the culture mediums to support the development**.** These recombinant human proteins were supplemented with EGF and Rocki. For the first week, hiPSCs were differentiated into

eye field stem cells, thereby they had similar morphologies as in cells of the ocular cell differentiation method (Figure 29A). As the recombinant proteins were added to the culture medium, the differentiated cells had different morphologies than those observed in multi-zonal ocular cells. Budding structures were observed under the microscope starting on day 20, giving rise to branchial structures (Figure 29B). Without any supplemental molecules, the observation of branching structures took about 30 days with the multi-zonal ocular cell differentiation protocol (see **Section 4.1.,** Figure16). When compared to that technique, differentiation and development time for *in vitro* culture models is reduced by approximately 10 days using these stimulatory molecules.

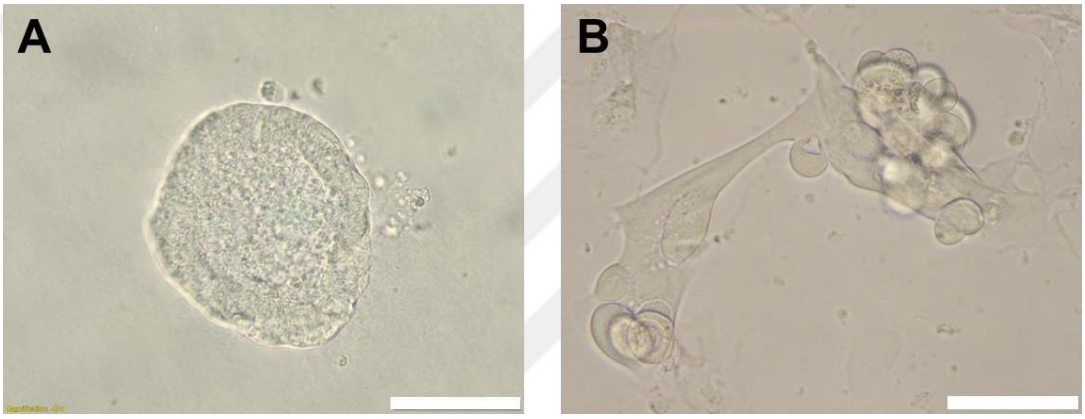

Figure 29. Stimulation of the branching morphogenesis on differentiating hiPSCs
BF images of the cultured cells A) on day 6, B) day 22. Scale bar: 100 µm

The control group (represented with ++), which has only EGF and Rocki, generally was not showed branching structures. Only some budding was observed in that group. On the other hand, in the remaining groups, which are supported with either FGF10, BMP7, or both, early branching morphogenesis was observed. Even though the culture was still highly heterogenic, most structures showed a glandular-like structure in culture. In comparison to the other groups, the group that was supported with both FGF10 and BMP7 had a higher number of these glandular-like structures (Figure 30).

At the end of 28 days, the expression of key genes for LG development and branching morphogenesis was examined via qPCR (Figure 31). SOX9 level was higher significantly in supported with FGF10 and BMP7 group compared to all the other groups indicating that our stimulation was successful to activate the main components

for the budding and branching morphogenesis. As SOX9 is activated through FGF signaling and is responsible for regulating main collagens, the expressions of FGF receptor 2 (FGFR2) and COL1A1 were investigated. FGFR2 expression was considerably higher in the supported with both recombinant proteins group, even higher than supported with only the FGF10 group, suggesting that FGF10 is more capable of activating branching when supported with BMP7. The expression of COL1A1 on the other hand, was almost similar for all the supported groups, higher than iPSCs. In contrast, MMP expressions, both MMP2 and MMP9 had no significant change compared to iPSCs when supported. PAX6 levels were significantly higher than iPSCs in the experimental group, implying CE differentiation can be supported through FGF10 and BMP7 supplementation.

Ductal markers such as AQP5 and LTF showed no significant change for the experimental groups interestingly. As an early LG development marker COL9A2, showed an increased expression in FGF10 and BMP7 supported groups and showed higher expression in the group that is supported by both factors. NDST1 was also investigated as it's one of the co-receptors for FGFR2 to induce bud growth, however, no significant change was observed (Figure 32).

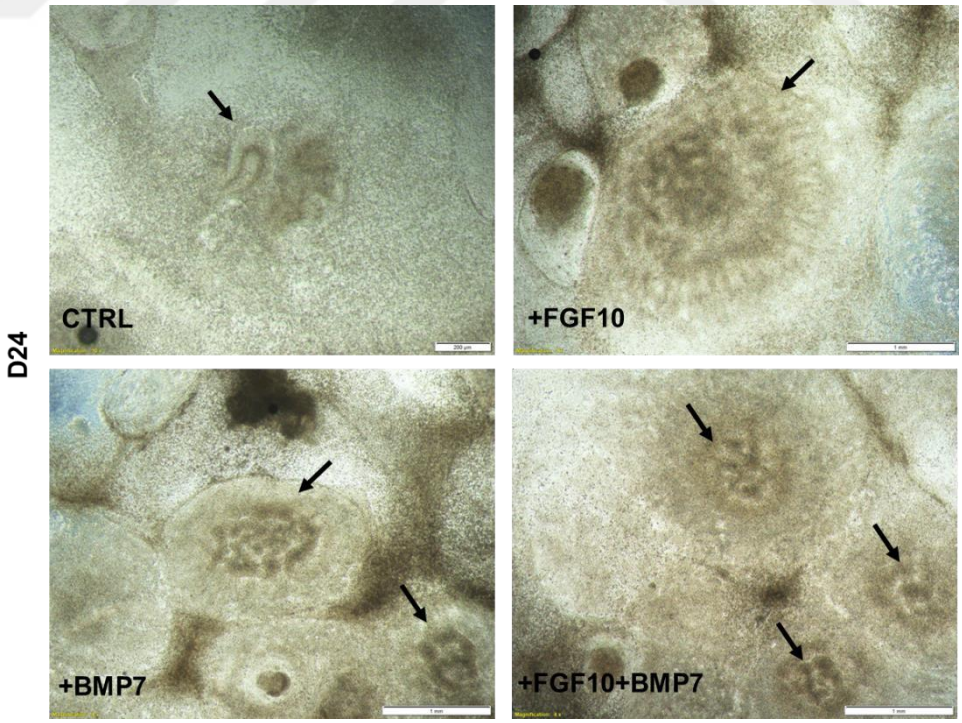

Figure 30. Differentiation with the stimulatory recombinant proteins
BF images on day 24. Black arrows showing branching morphogenesis in culture. ++: EGF, Rocki; +FGF10: EGF, Rocki, FGF10; +BMP7: EGF, Rocki, BMP7; ++++: EGF, Rocki; FGF10, BMP7. Scale bars: 200 µm and 1mm.

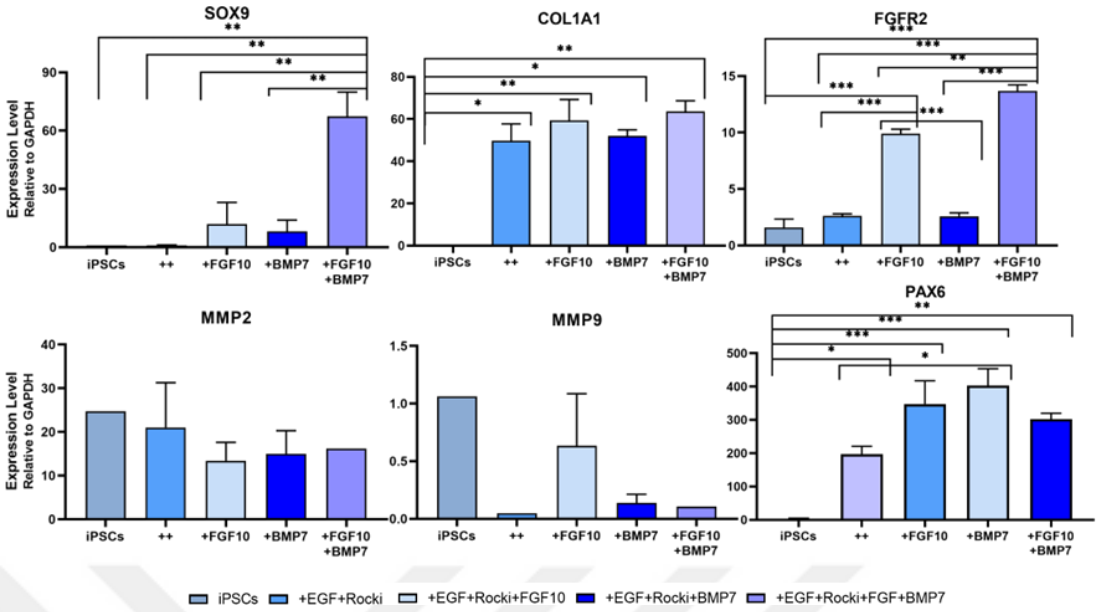

Figure 31. mRNA expression levels of key LG development genes in supported cells

SOX9, COL1A1 and FGFR2, MMP2, MMP9 and PAX6 mRNA expression levels in hiPSCs and differentiated ocular cells on 28 days. p<0.00005: ****, p<0.0005: ***, p<0.005: **,

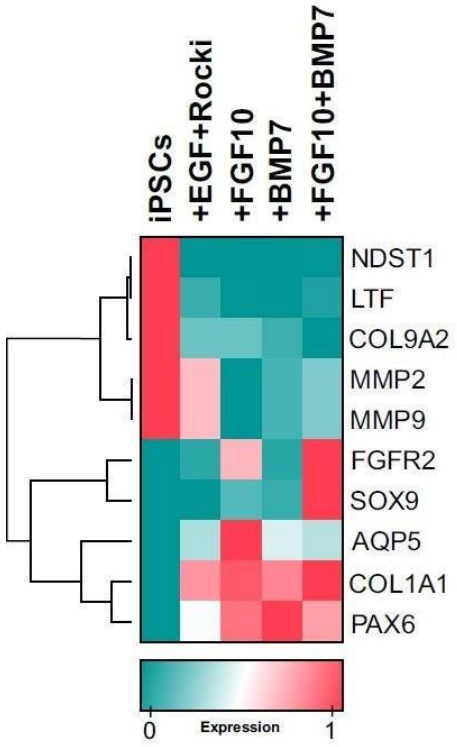

Figure 32. **Normalized gene expression levels of branching samples**
Heatmap showing gene expression levels in experimental groups. Expressions normalized and z-score implicated below.
p<0.5: *

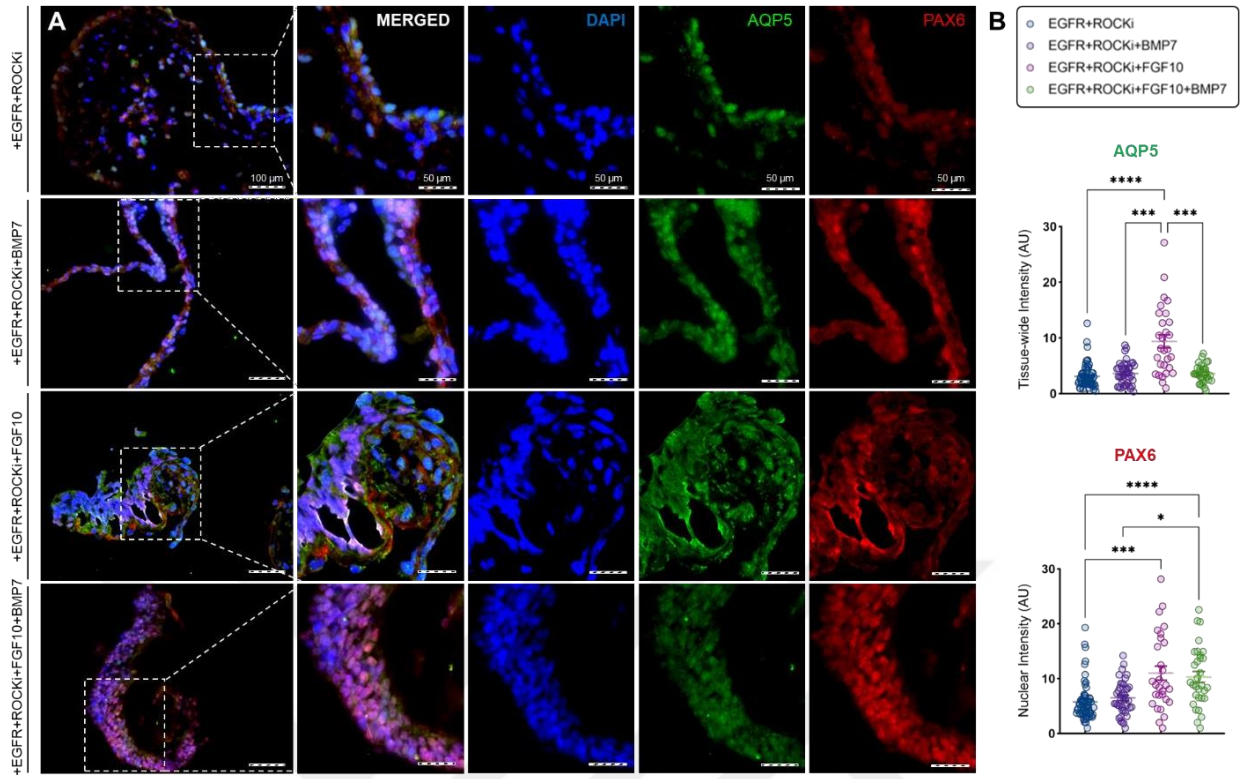

Figure 33. Fluorescence intensity of AQP5 and PAX6
For fluorescent intensity, all groups stained with same markers A) IF images of PAX6, AQP5 and DAPI. First column showed merged images, scale bar: 100 µm and rest of the columns merged, DAPI, red and green channels separately, scale bars 20 µm. B) Fluorescence intensity analysis of AQP5 and PAX6 (AU: arbitrary Unit). $p<0.00005$: ****, $p<0.0005$: ***, $p<0.005$: **, $p<0.5$: *

IF staining was performed for all the experimental groups to examine ductal and myoepithelial cell markers. The fluorescence intensity was calculated to compare the protein expression levels in different groups. According to the results, AQP5 expression was significantly higher in the FGF10 supported group whereas PAX6 expression was highest in the FGF10 and BMP7 supported group (Figure 33). Additionally, IF staining of PAX6 and E-cadherin indicated that, E-cadherin is highly expressed in the stimulated group with both supportive molecules (Figure 34).

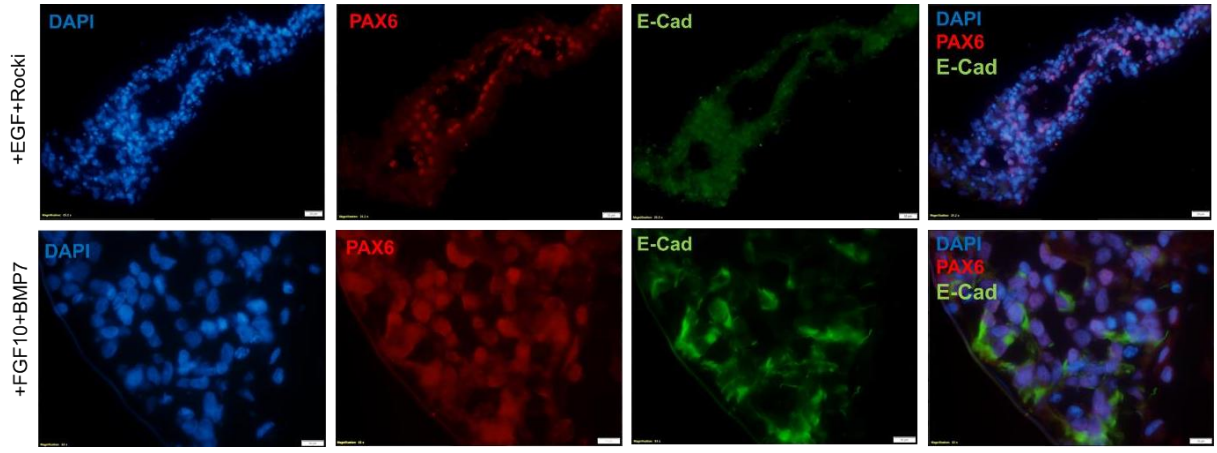

Figure 34. PAX6 and E-Cadherin protein expressions in branching samples
IF images of the control sample and stimulated sample showing PAX6 and E-Cadherin expression Scale bars: 10μm, 20μm.

Protein expression patterns of α-SMA and LTF proteins showed similarity in the branching control group with organoid models grown under static culture conditions. The α-SMA protein presented on the surrounds of the tissue while LTF was also found on the inner side. That similarity indicates that 3D static culturing conditions had a resemblance with the 2D control group conditions in terms of cell structure (Figure 35).

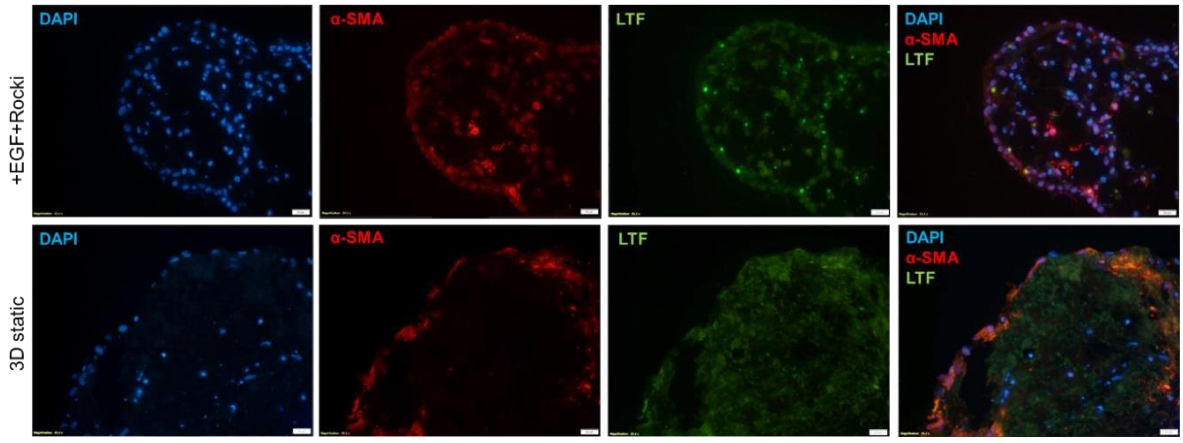

Figure 35. Protein expression patterns on branching control group and 3D sampled grown under static conditions
IF images of the control group and 3D static group samples showing α-SMA and LTF expressions. Scale bars: 20 μm.

Furthermore, the NAG activity assay was performed for branching samples to analyze the secretion functionality. Although the results did not show a significant change, the FGF10 stimulated group showed higher levels of activation in compare to the other groups (Figure 36).

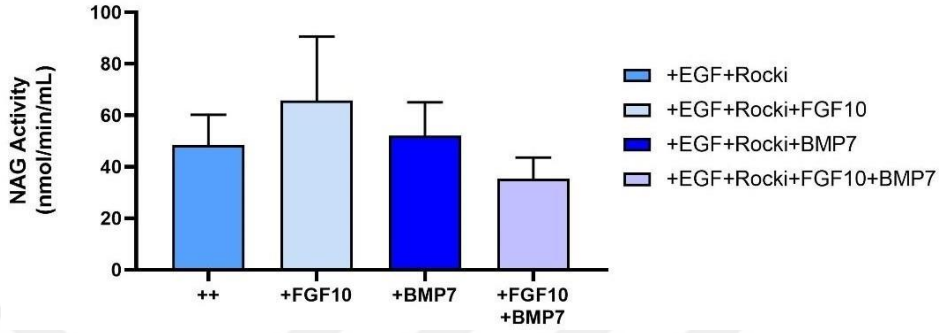

Figure 36. NAG Activity of branching samples

The organoids that grew under static and dynamic culture conditions were supported with branching supportive molecules while differentiating. IF staining was performed to analyze ductal cell marker lipocalin in the protein level. The results suggested that 3D branching samples showed the expression of LCN, which can be further modeled in improved conditions (Figure 37).

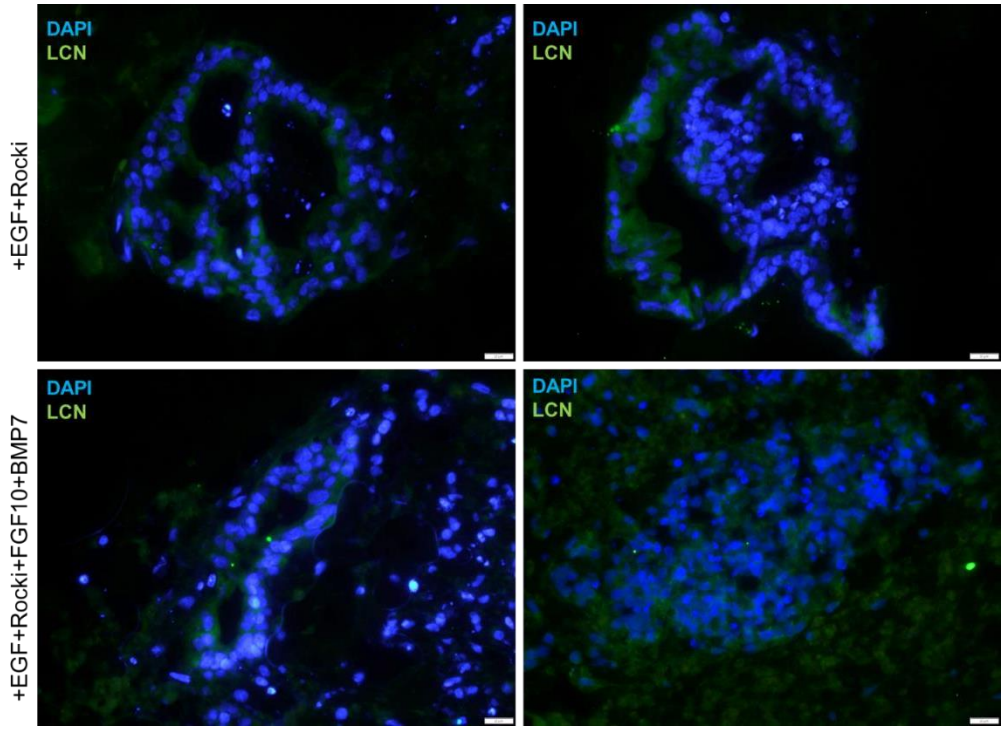

Figure 37. Lipocalin protein expression in 3D branching samples
IF images of control and stimulated groups showing LCN expression. Scale bar: 20 μm.

4.5. The metabolome of lacrimal gland organoids changes significantly under effect of different stimulants

A GC–MS-based metabolomic profiling investigation was performed in iPSC-derived lacrimal gland cells for fingerprint analysis. The experiment was run with 24 cell samples in total, 6 samples for each group. Multivariate statistical analysis employing partial least square discriminant analysis (PLS-DA) and heatmap was used to show metabolomic profiles (Figure 38). On day 28, metabolites from differentiated cells under the effect of different stimulants exhibited significant separation from each other (Figure 38 A). The metabolome shifting of distinct stimulant-applied cells demonstrates how stimulated samples respond to different stimulants (Figure 38 B).

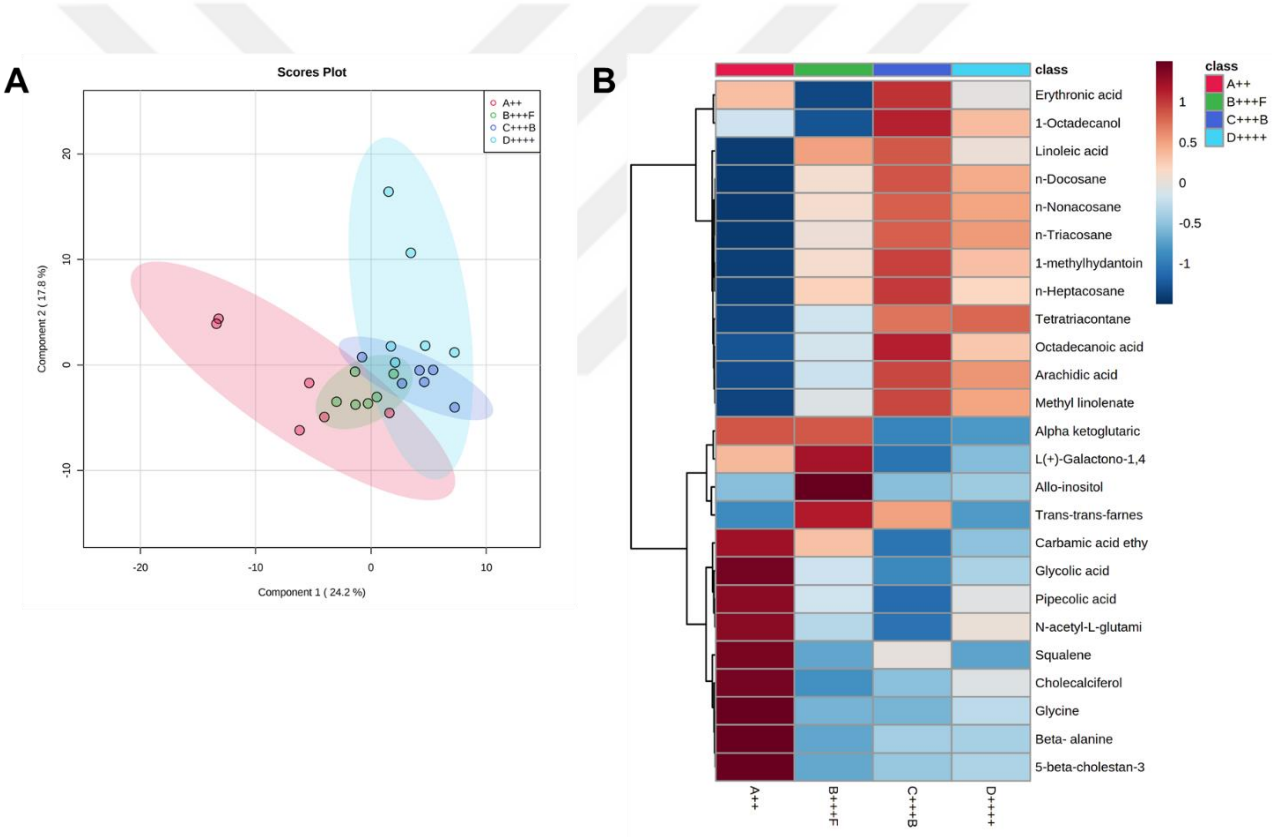

Figure 57. Metabolic analysis of branching cell samples
A) PLS-DA score plot for metabolomic profiles of cell lines at presence of the different stimulants; B) Heat map for group averages of cell metabolites. ++: EGF+Rocki; +++F: EGF+Rocki+FGF10; +++B: EGF+Rocki+BMP7; ++++: EGF+Rocki+FGF10+BMP7

5. DISCUSSION

The differentiation of hiPSCs to ocular cells was already performed by our lab as a previous study. However, because of the heterogeneity, the presence of LG markers was found together with other types of ocular cells, and the efficiency of the formation of LG structures was unfortunately low. In this thesis, methods have been developed and implied for increasing the efficiency of differentiation hiPSCs to LG cells. Different approaches have been tried to find the most effective way that results in functional LG models. For all of the experiments, Matrigel was used as a supportive ECM component which helps better support stem cell differentiation, as well as mimicking the native-like environment. Different components may differ in the results. Furthermore, in this study only the WT1-hiPSC cell line was used, other types of iPSC cell lines also can be evaluated.

5.1. hiPSC Differentiation to Lacrimal Gland Organoids

For inducing organoid formation, hiPSCs were seeded on Matrigel coated plates, which were used in the concentration of either 1% or 100%. As expected, 1% Matrigel did not support organoid differentiation from hiPSCs, since the ECM components are necessary for the proper development of cell architecture. Thereby, the coating was performed 100% Matrigel for all the culturing platforms including the microfluidic chips. For the top coating, 2% and 70% Matrigel concentrations were tested. Similar to surface coating, the lower concentration provided lower support to organoid formation. For that reason, cell seeding is followed by 70% Matrigel coating on top of the cells. After cell seeding, in the case of immediate induction of differentiation, cells did not show a differentiated morphology, and most of them died eventually. The ones who survived did not proliferate so; the organoid formation was not successfully achieved. As a potential solution, cells continue culturing with mTesR for 3 more days. In this way, while they were adjusting to the new environment, their pluripotent characteristics were maintained. At the end of 3 days, mTesR was replaced with the EDM and the differentiation was started.

For the organoids that are cultured under dynamic conditions, the duration of the flow was pivotal as its effect on sample attachment to the surface together with the

pressure and shear stress generated on the organoid models. To allow the organoids to adhere to the surface after the passage, the flow was not initiated immediately, all microchips were cultured under static conditions for 3 days. At first trials, the flow was administrated for 2 weeks, however, organoids were losing their integrity as well as cell viability under such dynamic conditions. Thereby, the flow was shortened to 1 week for all the experiments. For long-term cultures, reducing the flow rate could also be a potential solution.

All iPSC derived organoids have diverse properties since they came from a background with a heterogenic ocular cell population. Some organoids generated in this study had swelling compartments; some had gained integrity and gotten bigger in size while some had formed branchial structures. Nevertheless, within each group, the results were generally consistent. For example, the ones that are cultured under dynamic conditions were better attached to the surface, proliferate and form extensions. Here, the swelling compartment could be a key marker for the LG-organoids since its secretory function could be observed in culture as a swelling compartment. On the other hand, organoids cultured under static conditions were hardly attached to the surface, some shrunken and reduced in size. Only a few of them showed growing and proliferating features. In order to be precise, organoids could be divided by their morphologies, and only those who were observed as a potential LG-organoids -such as the ones with swelling compartment- could be passaged for further processes. However, the appearance of organoids with morphological similarities in culture is very low. For inducing the formation of more specific differentiation of organoids, cell sorting techniques could be useful. Thereby, similar organoids could be compared in different culturing platforms.

5.2. Maturated Ocular Cells Passaging to Microfluidic Platforms

After differentiation of hiPSCs to ocular cells, maturated samples passaged to the microfluidic platform to grow individually. The sample viability in this experimental set was much higher in comparison to the previous experimental set. That may be because the maturity of the samples affects their features even after passage. Almost all the samples continued to grow following the passage, which indicates our microfluidic design and culture conditions were proper for culture. A considerable amount of newly

attached cells apart from the sample was also grow and proliferated inside the platforms. That could be because of the presence of a higher number of cells, as mature tissues are larger compared to other 1-month-olds. Additionally, the expression of PAX6 and E-cad indicates that these samples are potential LG models. According to their morphologies, samples grown under dynamic conditions were better attached to the surface and gave rise to branchial structures by the supporting flow.

5.3. Branching Morphology Induction

According to literature and previous studies, FGF10 and BMP7 play a critical role in regulating branching morphogenesis of the human lacrimal gland. For increasing our differentiation protocols' efficiency, these molecules were added to the culture exogenously. After culturing with supplemental molecules, the expression of some downstream and upstream elements of FGF10 and BMP7 signaling were examined. As expected, FGFR2 expression levels were higher in the supported groups in comparison to the control group and iPSCs, indicating the receptor is successfully activated through the exogenous FGF10. The supported group with both recombinant proteins had considerably higher FGFR2 expression than the supported with only FGF10 group, implying that FGF10 is more capable of activating branching when supported with BMP7. SOX9 expression was also higher in the stimulated group with both FGF10 and BMP7, similarly to FGFR2. As its one of the main branching regulatory genes, its considerably high expression suggests that branching has been stimulated. Additionally, since MMPs are the downstream elements for FGF signaling, in the case of exogenous administration of FGF10, they did not demonstrate activation. Thereby, they had similar expression levels within iPSCs, as expected.

On the other hand, COL1A1 showed similar expression levels in all experimental groups. Other types of collagens such as COL2A1 could be investigated for more detailed analysis since it's the hallmark of nascent LG bud. The case was similar for the NDST1 gene, its expression did not show a significant change between experimental groups including the control group and iPSCs. However, since it's one of the co-receptor genes of FGFR2, other co-receptors such as HS2ST or HS6ST genes' expression could be investigated.

Moreover, the ductal marker AQP5 showed no significant change in the mRNA expression level whereas its expression at the protein level was the highest in the FGF10 supported group. Further analyze could perform via western blotting to confirm its presence and intensity. Similarly, the LTF mRNA expression levels were almost the same for all the experimental groups. It could also be detected via ELISA or western blotting for more precise analysis.

The culture was extended for 28 days for this experimental design. Culture duration could be extended more to examine the changes in the expression of key LG-related gene markers.

6. CONCLUSION and FUTURE DIRECTIONS

In conclusion, it has been shown by this research that, iPSCs can be differentiated into ocular organoids and more specifically, potential LG organoids that can grow under dynamic conditions *in vitro*. Microfluidic platforms used for culturing the samples in 3D supported with Matrigel, creating a more native-like environment, and allowing development under flow similar to tissues in the body. Characteristics of developed ocular samples showed similarity with human LG, in terms of key marker expression and secretion function. Furthermore, expression of LGR5 and β-Catenin was detected in the samples indicating their role in LG morphogenesis. More studies could perform focusing on this pathway to enlighten their regulatory potential on the differentiation. Moreover, microfluidic platforms could be improved in future studies, and serve as a potential platform for therapeutic approaches such as drug discoveries.

Additionally, exogenous stimulatory factors FGF10 and BMP7 were used for *in vitro* recapitulating budding and branching morphogenesis of human LG. According to the results of expression analyses, stimulation induced by these exogenous molecules and activated signaling pathways that play main roles in branching morphogenesis. These results were very promising for inducing LG formation and decreasing heterogeneity in our ocular cell differentiation protocol. In future studies, heterogeneity may be prevented by cell sorting and the differentiation to LG could be more stimulated via these molecules.

Since both approaches were promising, they could be combined together. So that, stimulation could be performed on samples in microfluidic platforms under dynamic conditions. Development of more functional LG organoid models could be developed by this method.

7. REFERENCES

A, L., Yx, W., Y, J., C, B., Jb, J., & L, X. (2013). Dry eye disease, dry eye symptoms and depression: The Beijing Eye Study. *The British Journal of Ophthalmology*, *97*(11). https://doi.org/10.1136/bjophthalmol-2013-303838

Akbari, S., Sevinç, G. G., Ersoy, N., Basak, O., Kaplan, K., Sevinç, K., Ozel, E., Sengun, B., Enustun, E., Ozcimen, B., Bagriyanik, A., Arslan, N., Önder, T. T., & Erdal, E. (2019). Robust, Long-Term Culture of Endoderm-Derived Hepatic Organoids for Disease Modeling. *Stem Cell Reports*, *13*(4), 627–641. https://doi.org/10.1016/j.stemcr.2019.08.007

Bai, Q., Desprat, R., Klein, B., Lemaitre, J.-M., & De Vos, J. (2013). Embryonic stem cells or induced pluripotent stem cells? A DNA integrity perspective. *Current Gene Therapy*, *13*(2), 93–98.

Bannier-Hélaouët, M., Post, Y., Korving, J., Trani Bustos, M., Gehart, H., Begthel, H., Bar-Ephraim, Y. E., van der Vaart, J., Kalmann, R., Imhoff, S. M., & Clevers, H. (2021). Exploring the human lacrimal gland using organoids and single-cell sequencing. *Cell Stem Cell*, *28*(7), 1221-1232.e7. https://doi.org/10.1016/j.stem.2021.02.024

Bron, A. J., de Paiva, C. S., Chauhan, S. K., Bonini, S., Gabison, E. E., Jain, S., Knop, E., Markoulli, M., Ogawa, Y., Perez, V., Uchino, Y., Yokoi, N., Zoukhri, D., & Sullivan, D. A. (2017). TFOS DEWS II pathophysiology report. *The Ocular Surface*, *15*(3), 438–510. https://doi.org/10.1016/j.jtos.2017.05.011

Celebi, A. R. C., Ulusoy, C., & Mirza, G. E. (2014). The efficacy of autologous serum eye drops for severe dry eye syndrome: A randomized double-blind crossover study. *Graefe's Archive for Clinical and Experimental Ophthalmology = Albrecht Von Graefes Archiv Fur Klinische Und Experimentelle Ophthalmologie*, *252*(4), 619–626. https://doi.org/10.1007/s00417-014-2599-1

Chagastelles, P. C., & Nardi, N. B. (2011). Biology of stem cells: An overview. *Kidney International Supplements*, *1*(3), 63–67. https://doi.org/10.1038/kisup.2011.15

Chen, Z., Huang, J., Liu, Y., Dattilo, L. K., Huh, S.-H., Ornitz, D., & Beebe, D. C. (2014). FGF signaling activates a Sox9-Sox10 pathway for the formation and branching morphogenesis of mouse ocular glands. *Development (Cambridge, England)*, *141*(13), 2691–2701. https://doi.org/10.1242/dev.108944

Chin, M. H., Pellegrini, M., Plath, K., & Lowry, W. E. (2010). Molecular analyses of human induced pluripotent stem cells and embryonic stem cells. *Cell Stem Cell*, *7*(2), 263–269. https://doi.org/10.1016/j.stem.2010.06.019

Clevers, H. (2016). Modeling Development and Disease with Organoids. *Cell*, *165*(7), 1586–1597. https://doi.org/10.1016/j.cell.2016.05.082

Conrady, C. D., Joos, Z. P., & Patel, B. C. K. (2016). Review: The Lacrimal Gland and Its Role in Dry Eye. *Journal of Ophthalmology*, *2016*, 7542929. https://doi.org/10.1155/2016/7542929

Craig, J. P., Nichols, K. K., Akpek, E. K., Caffery, B., Dua, H. S., Joo, C.-K., Liu, Z., Nelson, J. D., Nichols, J. J., Tsubota, K., & Stapleton, F. (2017). TFOS DEWS II Definition and Classification Report. *The Ocular Surface*, *15*(3), 276–283. https://doi.org/10.1016/j.jtos.2017.05.008

Daley, W. P., & Yamada, K. M. (2013). ECM-modulated cellular dynamics as a driving force for tissue morphogenesis. *Current Opinion in Genetics & Development*, *23*(4), 408–414. https://doi.org/10.1016/j.gde.2013.05.005

Dartt, D. A. (2009). Neural regulation of lacrimal gland secretory processes: Relevance in dry eye diseases. *Progress in Retinal and Eye Research*, *28*(3), 155–177. https://doi.org/10.1016/j.preteyeres.2009.04.003

de la Cuadra-Blanco, C., Peces-Peña, M. D., & Mérida-Velasco, J. R. (2003). Morphogenesis of the human lacrimal gland. *Journal of Anatomy*, *203*(5), 531–536. https://doi.org/10.1046/j.1469-7580.2003.00233.x

Dean, C. H., Miller, L.-A. D., Smith, A. N., Dufort, D., Lang, R. A., & Niswander, L. A. (2005). Canonical Wnt signaling negatively regulates branching morphogenesis of the lung and lacrimal gland. *Developmental Biology*, *286*(1), 270–286. https://doi.org/10.1016/j.ydbio.2005.07.034

Dean, C., Ito, M., Makarenkova, H. P., Faber, S. C., & Lang, R. A. (2004). Bmp7 regulates branching morphogenesis of the lacrimal gland by promoting mesenchymal proliferation and condensation. *Development (Cambridge, England)*, *131*(17), 4155–4165. https://doi.org/10.1242/dev.01285

Dietrich, J., & Schrader, S. (2020). Towards Lacrimal Gland Regeneration: Current Concepts and Experimental Approaches. *Current Eye Research*, *45*(3), 230–240. https://doi.org/10.1080/02713683.2019.1637438

Doane, M. G. (1981). Blinking and the mechanics of the lacrimal drainage system. *Ophthalmology*, *88*(8), 844–851. https://doi.org/10.1016/s0161-6420(81)34940-9

Doi, A., Park, I.-H., Wen, B., Murakami, P., Aryee, M. J., Irizarry, R., Herb, B., Ladd-Acosta, C., Rho, J., Loewer, S., Miller, J., Schlaeger, T., Daley, G. Q., & Feinberg, A. P. (2009). Differential methylation of tissue- and cancer-specific CpG island shores distinguishes human induced pluripotent stem cells, embryonic stem cells and fibroblasts. *Nature Genetics*, *41*(12), 1350–1353. https://doi.org/10.1038/ng.471

Donthineni, P. R., Kammari, P., Shanbhag, S. S., Singh, V., Das, A. V., & Basu, S. (2019). Incidence, demographics, types and risk factors of dry eye disease in India: Electronic medical records driven big data analytics report I. *The Ocular Surface*, *17*(2), 250–256. https://doi.org/10.1016/j.jtos.2019.02.007

Downie, L. E., Bandlitz, S., Bergmanson, J. P. G., Craig, J. P., Dutta, D., Maldonado-Codina, C., Ngo, W., Siddireddy, J. S., & Wolffsohn, J. S. (2021). CLEAR - Anatomy and physiology of the anterior eye. *Contact Lens & Anterior Eye: The Journal of the British Contact Lens Association*, *44*(2), 132–156. https://doi.org/10.1016/j.clae.2021.02.009

Garg, A., & Zhang, X. (2017). Lacrimal gland development: From signaling interactions to regenerative medicine. *Developmental Dynamics: An Official Publication of the American Association of Anatomists*, *246*(12), 970–980. https://doi.org/10.1002/dvdy.24551

Gromova, A., Voronov, D. A., Yoshida, M., Thotakura, S., Meech, R., Dartt, D. A., & Makarenkova, H. P. (2017). Lacrimal Gland Repair Using Progenitor Cells. *Stem Cells Translational Medicine*, *6*(1), 88–98. https://doi.org/10.5966/sctm.2016-0191

Guenther, M. G., Frampton, G. M., Soldner, F., Hockemeyer, D., Mitalipova, M., Jaenisch, R., & Young, R. A. (2010). Chromatin structure and gene expression programs of human embryonic and induced pluripotent stem cells. *Cell Stem Cell*, *7*(2), 249–257. https://doi.org/10.1016/j.stem.2010.06.015

Hayashi, R., Okubo, T., Kudo, Y., Ishikawa, Y., Imaizumi, T., Suzuki, K., Shibata, S., Katayama, T., Park, S.-J., Young, R. D., Quantock, A. J., & Nishida, K. (2022).

Generation of 3D lacrimal gland organoids from human pluripotent stem cells. *Nature*, *605*(7908), 126–131. https://doi.org/10.1038/s41586-022-04613-4

Hirayama, M., Kawakita, T., Tsubota, K., & Shimmura, S. (2016). Challenges and Strategies for Regenerating the Lacrimal Gland. *The Ocular Surface*, *14*(2), 135–143. https://doi.org/10.1016/j.jtos.2015.11.005

Hirayama, M., Ogawa, M., Oshima, M., Sekine, Y., Ishida, K., Yamashita, K., Ikeda, K., Shimmura, S., Kawakita, T., Tsubota, K., & Tsuji, T. (2013). Functional lacrimal gland regeneration by transplantation of a bioengineered organ germ. *Nature Communications*, *4*(1), 2497. https://doi.org/10.1038/ncomms3497

Hirayama, M., Tsubota, K., & Tsuji, T. (2015). Bioengineered Lacrimal Gland Organ Regeneration in Vivo. *Journal of Functional Biomaterials*, *6*(3), 634–649. https://doi.org/10.3390/jfb6030634

Hodges, R. R., & Dartt, D. A. (2003). Regulatory pathways in lacrimal gland epithelium. *International Review of Cytology*, *231*, 129–196. https://doi.org/10.1016/s0074-7696(03)31004-6

Holly, F. J., & Lemp, M. A. (1977). Tear physiology and dry eyes. *Survey of Ophthalmology*, *22*(2), 69–87. https://doi.org/10.1016/0039-6257(77)90087-x

Jeong, S. Y., Choi, W. H., Jeon, S. G., Lee, S., Park, J.-M., Park, M., Lee, H., Lew, H., & Yoo, J. (2021). Establishment of functional epithelial organoids from human lacrimal glands. *Stem Cell Research & Therapy*, *12*(1), 247. https://doi.org/10.1186/s13287-021-02133-y

Johnson, M. E., & Murphy, P. J. (2004). Changes in the tear film and ocular surface from dry eye syndrome. *Progress in Retinal and Eye Research*, *23*(4), 449–474. https://doi.org/10.1016/j.preteyeres.2004.04.003

Johnston, M. C., Noden, D. M., Hazelton, R. D., Coulombre, J. L., & Coulombre, A. J. (1979). Origins of avian ocular and periocular tissues. *Experimental Eye Research*, *29*(1), 27–43. https://doi.org/10.1016/0014-4835(79)90164-7

Kammandel, B., Chowdhury, K., Stoykova, A., Aparicio, S., Brenner, S., & Gruss, P. (1999). Distinct cis-essential modules direct the time-space pattern of the Pax6 gene activity. *Developmental Biology*, *205*(1), 79–97. https://doi.org/10.1006/dbio.1998.9128

Kim, H. Y., & Nelson, C. M. (2012). Extracellular matrix and cytoskeletal dynamics during branching morphogenesis. *Organogenesis*, *8*(2), 56–64. https://doi.org/10.4161/org.19813

Kolios, G., & Moodley, Y. (2013). Introduction to stem cells and regenerative medicine. *Respiration; International Review of Thoracic Diseases*, *85*(1), 3–10. https://doi.org/10.1159/000345615

Kumar, K. K., Burgess, A. W., & Gulbis, J. M. (2014). Structure and function of LGR5: An enigmatic G-protein coupled receptor marking stem cells. *Protein Science: A Publication of the Protein Society*, *23*(5), 551–565. https://doi.org/10.1002/pro.2446

Landry, D. W., & Zucker, H. A. (2004). Embryonic death and the creation of human embryonic stem cells. *The Journal of Clinical Investigation*, *114*(9), 1184–1186. https://doi.org/10.1172/JCI23065

Langer, R., & Vacanti, J. P. (1993). Tissue engineering. *Science (New York, N.Y.)*, *260*(5110), 920–926. https://doi.org/10.1126/science.8493529

Lemp, M. A., Crews, L. A., Bron, A. J., Foulks, G. N., & Sullivan, B. D. (2012). Distribution of aqueous-deficient and evaporative dry eye in a clinic-based patient cohort: A retrospective study. *Cornea*, *31*(5), 472–478. https://doi.org/10.1097/ICO.0b013e318225415a

Li, Z., Duan, H., Li, W., Hu, X., Jia, Y., Zhao, C., Zhang, S., Zhou, Q., & Shi, W. (2019). Rapid Differentiation of Multi-Zone Ocular Cells from Human Induced Pluripotent Stem Cells and Generation of Corneal Epithelial and Endothelial Cells. *Stem Cells and Development*, *28*(7), 454–463. https://doi.org/10.1089/scd.2018.0176

Lin, H., Sun, G., He, H., Botsford, B., Li, M., Elisseeff, J. H., & Yiu, S. C. (2016). Three-Dimensional Culture of Functional Adult Rabbit Lacrimal Gland Epithelial Cells on Decellularized Scaffold. *Tissue Engineering. Part A*, *22*(1–2), 65–74. https://doi.org/10.1089/ten.TEA.2015.0286

Lu, Q., Yin, H., Grant, M. P., & Elisseeff, J. H. (2017). An In Vitro Model for the Ocular Surface and Tear Film System. *Scientific Reports*, *7*(1), 6163. https://doi.org/10.1038/s41598-017-06369-8

Makarenkova, H. P., & Dartt, D. A. (2015). Myoepithelial Cells: Their Origin and Function in Lacrimal Gland Morphogenesis, Homeostasis, and Repair. *Current Molecular Biology Reports*, *1*(3), 115–123.

Makarenkova, H. P., Hoffman, M. P., Beenken, A., Eliseenkova, A. V., Meech, R., Tsau, C., Patel, V. N., Lang, R. A., & Mohammadi, M. (2009). Differential interactions of FGFs with heparan sulfate control gradient formation and branching morphogenesis. *Science Signaling*, *2*(88), ra55. https://doi.org/10.1126/scisignal.2000304

Makarenkova, H. P., Ito, M., Govindarajan, V., Faber, S. C., Sun, L., McMahon, G., Overbeek, P. A., & Lang, R. A. (2000). FGF10 is an inducer and Pax6 a competence factor for lacrimal gland development. *Development (Cambridge, England)*, *127*(12), 2563–2572.

Manafi, N., Shokri, F., Achberger, K., Hirayama, M., Mohammadi, M. H., Noorizadeh, F., Hong, J., Liebau, S., Tsuji, T., Quinn, P. M. J., & Mashaghi, A. (2021). Organoids and organ chips in ophthalmology. *The Ocular Surface*, *19*, 1–15. https://doi.org/10.1016/j.jtos.2020.11.004

Marinho, D. R., Burmann, T. G., & Kwitko, S. (2010). Labial salivary gland transplantation for severe dry eye due to chemical burns and Stevens-Johnson syndrome. *Ophthalmic Plastic and Reconstructive Surgery*, *26*(3), 182–184. https://doi.org/10.1097/IOP.0b013e3181b8c3ad

Mattiske, D., Sommer, P., Kidson, S. H., & Hogan, B. L. M. (2006). The role of the forkhead transcription factor, Foxc1, in the development of the mouse lacrimal gland. *Developmental Dynamics: An Official Publication of the American Association of Anatomists*, *235*(4), 1074–1080. https://doi.org/10.1002/dvdy.20702

Melis Asal. (2020). *Generation of lacrimal gland from induced pluripotent stem cells (Masters thesis, Dokuz Eylul University, 2020), Thesis ID:633320*. https://tez.yok.gov.tr/UlusalTezMerkezi/tezSorguSonucYeni.jsp

Messmer, E. M. (2015). The Pathophysiology, Diagnosis, and Treatment of Dry Eye Disease. *Deutsches Ärzteblatt International*, *112*(5), 71–82. https://doi.org/10.3238/arztebl.2015.0071

Mikkelsen, T. S., Hanna, J., Zhang, X., Ku, M., Wernig, M., Schorderet, P., Bernstein, B. E., Jaenisch, R., Lander, E. S., & Meissner, A. (2008). Dissecting direct reprogramming through integrative genomic analysis. *Nature*, *454*(7200), 49–55. https://doi.org/10.1038/nature07056

Mircheff, A. K. (1989). Lacrimal fluid and electrolyte secretion: A review. *Current Eye Research*, *8*(6), 607–617. https://doi.org/10.3109/02713688908995761

Nakao, K., Morita, R., Saji, Y., Ishida, K., Tomita, Y., Ogawa, M., Saitoh, M., Tomooka, Y., & Tsuji, T. (2007). The development of a bioengineered organ germ method. *Nature Methods*, *4*(3), 227–230. https://doi.org/10.1038/nmeth1012

Narsinh, K. H., Jia, F., Robbins, R. C., Kay, M. A., Longaker, M. T., & Wu, J. C. (2011). Generation of adult human induced pluripotent stem cells using nonviral minicircle DNA vectors. *Nature Protocols*, *6*(1), 78–88. https://doi.org/10.1038/nprot.2010.173

Nelson, J. D., Craig, J. P., Akpek, E. K., Azar, D. T., Belmonte, C., Bron, A. J., Clayton, J. A., Dogru, M., Dua, H. S., Foulks, G. N., Gomes, J. A. P., Hammitt, K. M., Holopainen, J., Jones, L., Joo, C.-K., Liu, Z., Nichols, J. J., Nichols, K. K., Novack, G. D., … Sullivan, D. A. (2017). TFOS DEWS II Introduction. *The Ocular Surface*, *15*(3), 269–275. https://doi.org/10.1016/j.jtos.2017.05.005

Obata, H. (2006). Anatomy and histopathology of the human lacrimal gland. *Cornea*, *25*(10 Suppl 1), S82-89. https://doi.org/10.1097/01.ico.0000247220.18295.d3

Okita, K., Nakagawa, M., Hyenjong, H., Ichisaka, T., & Yamanaka, S. (2008). Generation of mouse induced pluripotent stem cells without viral vectors. *Science (New York, N.Y.)*, *322*(5903), 949–953. https://doi.org/10.1126/science.1164270

O'Neil, E. C., Henderson, M., Massaro-Giordano, M., & Bunya, V. Y. (2019). Advances in Dry Eye Disease Treatment. *Current Opinion in Ophthalmology*, *30*(3), 166–178. https://doi.org/10.1097/ICU.0000000000000569

Patel, N., Sharpe, P. T., & Miletich, I. (2011). Coordination of epithelial branching and salivary gland lumen formation by Wnt and FGF signals. *Developmental Biology*, *358*(1), 156–167. https://doi.org/10.1016/j.ydbio.2011.07.023

Paulsen, F. P., & Berry, M. S. (2006). Mucins and TFF peptides of the tear film and lacrimal apparatus. *Progress in Histochemistry and Cytochemistry*, *41*(1), 1–53. https://doi.org/10.1016/j.proghi.2006.03.001

Pflugfelder, S. C., Jones, D., Ji, Z., Afonso, A., & Monroy, D. (1999). Altered cytokine balance in the tear fluid and conjunctiva of patients with Sjögren's syndrome keratoconjunctivitis sicca. *Current Eye Research*, *19*(3), 201–211. https://doi.org/10.1076/ceyr.19.3.201.5309

Qu, X., Pan, Y., Carbe, C., Powers, A., Grobe, K., & Zhang, X. (2012). Glycosaminoglycan-dependent restriction of FGF diffusion is necessary for lacrimal gland development. *Development (Cambridge, England)*, *139*(15), 2730–2739. https://doi.org/10.1242/dev.079236

Ramirez, J.-M., Bai, Q., Dijon-Grinand, M., Assou, S., Gerbal-Chaloin, S., Hamamah, S., & Vos, J. D. (2010). Human pluripotent stem cells: From biology to cell therapy. *World Journal of Stem Cells*, *2*(2), 24–33. https://doi.org/10.4252/wjsc.v2.i2.24

Sant' Anna, A. E. B. P. P., Hazarbassanov, R. M., de Freitas, D., & Gomes, J. Á. P. (2012). Minor salivary glands and labial mucous membrane graft in the treatment of severe symblepharon and dry eye in patients with Stevens-Johnson syndrome. *The British Journal of Ophthalmology*, *96*(2), 234–239. https://doi.org/10.1136/bjo.2010.199901

Sato, T., Vries, R. G., Snippert, H. J., van de Wetering, M., Barker, N., Stange, D. E., van Es, J. H., Abo, A., Kujala, P., Peters, P. J., & Clevers, H. (2009). Single Lgr5 stem cells build crypt-villus structures in vitro without a mesenchymal niche. *Nature*, *459*(7244), 262–265. https://doi.org/10.1038/nature07935

Seo, J., Byun, W. Y., Alisafaei, F., Georgescu, A., Yi, Y.-S., Massaro-Giordano, M., Shenoy, V. B., Lee, V., Bunya, V. Y., & Huh, D. (2019). Multiscale reverse engineering of the human ocular surface. *Nature Medicine*, *25*(8), 1310–1318. https://doi.org/10.1038/s41591-019-0531-2

Song, J. K., Lee, K., Park, H. Y., Hyon, J. Y., Oh, S.-W., Bae, W. K., Han, J.-S., Jung, S. Y., Um, Y. J., Lee, G.-H., & Yang, J. H. (2017). Efficacy of Carboxymethylcellulose and Hyaluronate in Dry Eye Disease: A Systematic

Review and Meta-Analysis. *Korean Journal of Family Medicine*, *38*(1), 2–7. https://doi.org/10.4082/kjfm.2017.38.1.2

Spaniol, K., Metzger, M., Roth, M., Greve, B., Mertsch, S., Geerling, G., & Schrader, S. (2015). Engineering of a Secretory Active Three-Dimensional Lacrimal Gland Construct on the Basis of Decellularized Lacrimal Gland Tissue. *Tissue Engineering. Part A*, *21*(19–20), 2605–2617. https://doi.org/10.1089/ten.TEA.2014.0694

Stapleton, F., Alves, M., Bunya, V. Y., Jalbert, I., Lekhanont, K., Malet, F., Na, K.-S., Schaumberg, D., Uchino, M., Vehof, J., Viso, E., Vitale, S., & Jones, L. (2017). TFOS DEWS II Epidemiology Report. *The Ocular Surface*, *15*(3), 334–365. https://doi.org/10.1016/j.jtos.2017.05.003

Su, J.-Z., Cai, Z.-G., & Yu, G.-Y. (2015). Microvascular autologous submandibular gland transplantation in severe cases of keratoconjunctivitis sicca. *Maxillofacial Plastic and Reconstructive Surgery*, *37*(1). https://doi.org/10.1186/s40902-015-0006-4

Sullivan, D. A. (2004). Tearful relationships? Sex, hormones, the lacrimal gland, and aqueous-deficient dry eye. *The Ocular Surface*, *2*(2), 92–123. https://doi.org/10.1016/s1542-0124(12)70147-7

Takahashi, K., Tanabe, K., Ohnuki, M., Narita, M., Ichisaka, T., Tomoda, K., & Yamanaka, S. (2007a). Induction of pluripotent stem cells from adult human fibroblasts by defined factors. *Cell*, *131*(5), 861–872. https://doi.org/10.1016/j.cell.2007.11.019

Takahashi, K., Tanabe, K., Ohnuki, M., Narita, M., Ichisaka, T., Tomoda, K., & Yamanaka, S. (2007b). Induction of pluripotent stem cells from adult human fibroblasts by defined factors. *Cell*, *131*(5), 861–872. https://doi.org/10.1016/j.cell.2007.11.019

Takahashi, K., & Yamanaka, S. (2006). Induction of pluripotent stem cells from mouse embryonic and adult fibroblast cultures by defined factors. *Cell*, *126*(4), 663–676. https://doi.org/10.1016/j.cell.2006.07.024

Tiwari, S., Ali, M. J., & Vemuganti, G. K. (2014). Human lacrimal gland regeneration: Perspectives and review of literature. *Saudi Journal of Ophthalmology: Official*

Journal of the Saudi Ophthalmological Society, *28*(1), 12–18. https://doi.org/10.1016/j.sjopt.2013.09.004

Tiwari, S., Nair, R. M., Vamadevan, P., Ali, M. J., Naik, M. N., Honavar, S. G., & Vemuganti, G. K. (2018). Establishing and characterizing lacrispheres from human lacrimal gland for potential clinical application. *Graefe's Archive for Clinical and Experimental Ophthalmology = Albrecht Von Graefes Archiv Fur Klinische Und Experimentelle Ophthalmologie*, *256*(4), 717–727. https://doi.org/10.1007/s00417-018-3926-8

Tsau, C., Ito, M., Gromova, A., Hoffman, M. P., Meech, R., & Makarenkova, H. P. (2011). Barx2 and Fgf10 regulate ocular glands branching morphogenesis by controlling extracellular matrix remodeling. *Development (Cambridge, England)*, *138*(15), 3307–3317. https://doi.org/10.1242/dev.066241

Tsubota, K., Satake, Y., & Shimazaki, J. (1996). Treatment of severe dry eye. *The Lancet*, *348*(9020), 123. https://doi.org/10.1016/S0140-6736(96)24028-0

Walcott, B. (1998). The Lacrimal Gland and Its Veil of Tears. *News in Physiological Sciences: An International Journal of Physiology Produced Jointly by the International Union of Physiological Sciences and the American Physiological Society*, *13*, 97–103. https://doi.org/10.1152/physiologyonline.1998.13.2.97

Wan, Y., Zhang, M., & Li, X. (2019). *The global prevalence of dry eye disease and its association with economy: A systematic revie*. https://doi.org/10.21203/rs.2.10986/v1

Warren, L., Manos, P. D., Ahfeldt, T., Loh, Y.-H., Li, H., Lau, F., Ebina, W., Mandal, P. K., Smith, Z. D., Meissner, A., Daley, G. Q., Brack, A. S., Collins, J. J., Cowan, C., Schlaeger, T. M., & Rossi, D. J. (2010). Highly efficient reprogramming to pluripotency and directed differentiation of human cells with synthetic modified mRNA. *Cell Stem Cell*, *7*(5), 618–630. https://doi.org/10.1016/j.stem.2010.08.012

Wieczorek, R., Jakobiec, F. A., Sacks, E. H., & Knowles, D. M. (1988). The immunoarchitecture of the normal human lacrimal gland. Relevancy for understanding pathologic conditions. *Ophthalmology*, *95*(1), 100–109. https://doi.org/10.1016/s0161-6420(88)33228-8

Xiao, S., & Zhang, Y. (2020). Establishment of long-term serum-free culture for lacrimal gland stem cells aiming at lacrimal gland repair. *Stem Cell Research & Therapy*, *11*(1), 20. https://doi.org/10.1186/s13287-019-1541-1

Xinaris, C., Brizi, V., & Remuzzi, G. (2015). Organoid Models and Applications in Biomedical Research. *Nephron*, *130*(3), 191–199. https://doi.org/10.1159/000433566

Yao, Y., & Zhang, Y. (2017). The lacrimal gland: Development, wound repair and regeneration. *Biotechnology Letters*, *39*(7), 939–949. https://doi.org/10.1007/s10529-017-2326-1

Ye, L., Swingen, C., & Zhang, J. (2013). Induced Pluripotent Stem Cells and Their Potential for Basic and Clinical Sciences. *Current Cardiology Reviews*, *9*(1), 63–72. https://doi.org/10.2174/157340313805076278

Zoukhri, D., Fix, A., Alroy, J., & Kublin, C. L. (2008). Mechanisms of Murine Lacrimal Gland Repair after Experimentally Induced Inflammation. *Investigative Ophthalmology & Visual Science*, *49*(10), 4399–4406. https://doi.org/10.1167/iovs.08-1730

8. APPENDIX

8.1. Ethics Committee Approval

İZMİR BİYOTIP VE GENOM MERKEZİ
GİRİŞİMSEL OLMAYAN ARAŞTIRMALAR ETİK KURULU (İBG-GOEK)
KARARI

Toplantı Tarihi	: 26/07/2021	**Toplantı Günü**	: Pazartesi
Toplantı Sayısı	: 8	**Toplantı Saati**	: 10:30

Sayın Doç. Dr. Sinan GÜVEN,

2021-021 Protokol No'lu; sorumlusu olduğunuz "İnsan indüklenmiş pluripotent kök hücre kaynaklı lakrimal bez organoidlerinin farklılaşma verimliliğinin arttırılması" başlıklı araştırmanın uygulanmasında etik açıdan sakınca olmadığına oy birliği ile karar verilmiştir.

Bilgilerinizi ve gereğini rica ederiz.

Prof. Dr. H. Alper BAĞRIYANIK **Başkan** (Katılmadı)	**Dr. Serap ERKEK ÖZHAN** **Başkan Yardımcısı**
Prof. Dr. Sedef AKGÜNGÖR **Üye**	**Prof. Dr. İnci ALACACIOĞLU** **Üye**
Prof. Dr. Gülgün OKTAY **Üye** (Katılmadı)	**Prof. Dr. Hilmi ORHAN** **Üye**
Prof. Dr. Şermin GENÇ **Üye** (Katılmadı)	**Doç. Dr. Canan Aslı YILDIRIM** **Üye** (Katılmadı)
Doç. Dr. Can KÜÇÜK **Üye**	**Dr. Öğr. Üyesi Yavuz OKTAY** **Üye**

8.2. Cirruculum Vitae

Sude Uyulgan

ID Number:	
Date of Birth:	
Contact Address:	
Phone :	
e-mail:	

EDUCATIONAL BACKGROUND

Country	University	Faculty/ Institute	Department	Degree	Year of Graduation
Turkey	Izmir University of Economics	Engineering	Genetics and Bioengineering	Bachelor's	2020
Turkey	Dokuz Eylul University	Izmir Biomedicine and Genome Institute	Molecular Biology and Genetics	Master of Science	2022

ACADEMIC / PROFESSIONAL EXPERIENCE

Institution	Country	City	Department	Position	Year
Multigen, Teknopark, Ege University	Turkey	Izmir	Medical Biology	Internship	July 2018
University of Leipzig	Germany	Leipzig	Genetics	Internship	July 2019

SPECIALIZED FIELDS

Lacrimal Gland, Induced Pluripotent Stem Cells, Tissue Engineering, Regenerative Medicine